

THESIS

CONVECTIVE COLD POOLS: CHARACTERIZATION AND SOIL MOISTURE  
DEPENDENCE

Submitted by

Aryeh Jacob Drager

Department of Atmospheric Science

In partial fulfillment of the requirements

For the Degree of Master of Science

Colorado State University

Fort Collins, Colorado

Fall 2016

Master's Committee:

Advisor: Susan C. van den Heever

Christopher A. Davis

Michael J. Kirby

Wayne H. Schubert

Copyright by Aryeh Jacob Drager 2016

All Rights Reserved

## ABSTRACT

### CONVECTIVE COLD POOLS: CHARACTERIZATION AND SOIL MOISTURE DEPENDENCE

Convective cold pools play an important role in Earth's climate system. However, a common framework does not exist for conceptually defining and objectively identifying convective cold pools in observations and models. The first part of this thesis begins with a review of the identification methods used in previous works. This is followed by an investigation of convective cold pools within a high-resolution simulation of rainforest convection simulated using the Regional Atmospheric Modeling System (RAMS), an open-source cloud-resolving model with a coupled land-surface model. Multiple variables are assessed for their potential for identifying convective cold pool boundaries, and a novel technique is developed and tested for identifying and tracking convective cold pools in numerical model simulations. This algorithm is based on surface rainfall rates and radial gradients in the density potential temperature field. The algorithm successfully identifies near-surface cold pool boundaries and is able to distinguish between connected cold pools. Once cold pools have been identified and tracked, composites of cold pool evolution are then constructed, and average cold pool properties are investigated. One novel result is the presence of moist patches that develop within the centers of cold pools where the ground has been soaked with rainwater. These moist patches help to maintain cool temperatures and prevent cold pool dissipation, which has implications for the development of subsequent convection.

The second part of this thesis explores how the properties of convective cold pools are modulated by soil moisture. Three high-resolution simulations of tropical rainforest convection are performed using the RAMS, and the initial soil moisture is varied between 25% and 75% saturation. The cold pool identification algorithm developed in the first part of the thesis is used to construct composites of cold pools within each simulation, and the composites are compared. When soil moisture is decreased, stronger convective cold pools result. These stronger cold pools are also smaller because increased sensible heat fluxes in the reduced soil-moisture simulations cause the cold pools to dissipate more quickly as they expand. Finally, the rings of enhanced water vapor that have been documented in previous studies of tropical cold pools disappear when soil moisture is reduced. These results emphasize the role that land surface properties can have in modulating convective cold pool properties.

## ACKNOWLEDGEMENTS

This work has benefited from the contributions of many individuals. Firstly, I would like to acknowledge my advisor, Prof. Susan C. van den Heever, for overseeing this work and providing helpful guidance along the way. Over the course of this process, Prof. van den Heever has held me to high standards and has helped me become a sharper thinker and a more focused scientist. I am grateful to have her as my advisor. I would also like to acknowledge my committee members, Dr. Christopher A. Davis, Prof. Michael Kirby, and Prof. Wayne H. Schubert, for their insights and for their support and patience. I would furthermore like to acknowledge Leah Grant for performing and providing the simulations analyzed in this work.

This work also benefited from discussions I have had with members of the van den Heever Group, past and present, as well as with others at CSU. I would particularly like to acknowledge Steve Brey, Michal Clavner, Sean Freeman, Leah Grant, Steve Herbener, Adele Igel, Matt Igel, Peter Marinescu, Steve Saleeby, Amanda Sheffield, and Ben Toms for answering my questions, helping me overcome obstacles, and providing moral support. I would also like to acknowledge Matt Bishop and Ammon Redman for providing technical support. Finally, I would like to thank my mother, Jo Cohen, my father, Paul Drager, my grandmother, Marilyn Cohen, and my brother, Elon Drager for their love and support throughout this endeavor.

This work was funded in part by a graduate fellowship from the American Meteorological Society. It was also funded in part by the U.S. Department of Energy, Office of Science, Office of Biological and Environmental Research under Award Number DE-SC0010569. Finally, this work was supported in part by the National Science Foundation Graduate Research Fellowship Program under Grant No. DGE-1321845 Amend 5.

## TABLE OF CONTENTS

Abstract.....	ii
Acknowledgements.....	iv
Chapter 1: Introduction.....	1
1.1 Background.....	1
1.2 Goals.....	3
1.3 Methods.....	3
1.4 Thesis Structure.....	3
Chapter 2: Characterizing Convective Cold Pools.....	6
2.1 Introduction.....	6
2.2 Defining Cold Pools for Data Analysis.....	11
2.3 Model Setup.....	16
2.4 Choice of Variables.....	18
2.4.1 Buoyancy.....	19
2.4.2 Water Vapor Mixing Ratio.....	20
2.4.3 Equivalent Potential Temperature.....	21
2.4.4 Perturbation Pressure.....	21
2.4.5 Static Stability.....	22
2.4.6 Radial Velocity.....	22
2.4.7 Vertical Velocity.....	23
2.4.8 Surface Latent Heat Flux.....	24
2.4.9 Surface Sensible Heat Flux.....	25

2.4.10 Density Potential Temperature Advection.....	26
2.5 Algorithm for Cold Pool Identification and Tracking .....	26
2.5.1 Algorithm Development .....	26
2.5.2 Algorithm Performance .....	32
2.6 Composite Cold Pools .....	32
2.6.1 Overview.....	32
2.6.2 Moist Patch .....	35
2.7 Defining Cold Pool Depth .....	36
2.8 Summary and Conclusions .....	37
2.9 Table and Figures.....	40
Chapter 3: Soil Moisture Dependence .....	61
3.1 Introduction.....	61
3.2 Model Setup .....	63
3.3 Results.....	64
3.4 Discussion.....	69
3.5 Summary and Conclusions .....	70
3.6 Figures.....	71
Chapter 4: Concluding Remarks .....	75
4.1 Main Conclusions .....	75
4.2 Future Work .....	78
4.2.1 Algorithm Development .....	78
4.2.2 Further Cold Pool Studies.....	79
References.....	81

## CHAPTER 1: INTRODUCTION

### 1.1 Background

Convective cold pools are regions of near-surface, dense air that form in association with precipitating clouds. Downdrafts transport dry air from aloft down into the subcloud layer. As the air descends, precipitation evaporates, cooling the air. Evaporative cooling and hydrometeor loading combine to decrease the buoyancy of the downdraft air, and the resulting dense downdraft air collects at the surface, forming the cold pool. Upon reaching the ground, the cold pool air spreads out, forming a density current [e.g., Charba, 1974].

Cold pools have a role in the maintenance of long-lived squall lines [e.g., Rotunno *et al.*, 1988; Weisman and Rotunno, 2004] and in the formation of mesovortices [e.g., Wakimoto *et al.*, 2006]. Convective cold pools have also generated considerable interest due to their role in modulating convective organization [e.g., Tompkins, 2001; Jeevanjee and Romps, 2013a]. It is known that cold pools assist in generating new convection, but the processes by which they do so are not yet fully understood. Recent work [e.g., Tompkins, 2001; Torri *et al.*, 2015] points to two potential mechanisms. One mechanism, termed *mechanical forcing*, involves the lifting of near-surface environmental air by dense cold pool air wedging underneath it as the cold pool spreads out along the surface. Another mechanism, termed *thermodynamic forcing*, involves the generation of convective available potential energy (CAPE) and the erosion of convective inhibition (CIN) by surface sensible and latent heat fluxes into cold pool air (particularly cold pool air within the cold pool's outer regions, which accumulates these fluxes over the cold pool's entire lifetime) [e.g., Tompkins, 2001; Gentine *et al.*, 2016; Grant and van den Heever, 2016]. In both mechanisms, new convection is favored near the periphery of the cold pool.

According to the ingredients-based methodology of *Doswell* [1987], atmospheric moisture, conditional instability, and some lifting mechanism are all requirements for deep, moist convection. Mechanical forcing provides a lifting mechanism, whereas thermodynamic forcing provides conditional instability and moisture. Thus, although either forcing mechanism may promote the development of new convection, neither mechanism is necessarily sufficient on its own. If the two mechanisms coexist, and if additional mechanisms contribute to the triggering of new convection, the relative importance of each mechanism is unclear, as is the situational dependence (e.g., land versus ocean).

One approach to investigate convective cold pools and the processes by which they modulate convective organization is to track individual cold pools over their respective lifetimes. Such an approach allows composites to be constructed from collections of cold pools and also allows statistics to be calculated regarding various cold pool attributes. However, cold pool tracking is not a straightforward task, even in numerical simulations where all state variables, forcing terms, and time tendencies are known quantities. Cold pool boundaries often intersect, and new cold pools frequently form on the periphery of pre-existing cold pools [*Tompkins*, 2001; *Feng et al.*, 2015]. Cold pools also entrain environmental air, thus blurring the boundaries further, particularly in the vertical. Studies such as *Tompkins* [2001] have tracked cold pools manually; however, manual identification is impractical for large simulations and is subjective. Other studies have sought to develop automated, objective algorithms for cold pool tracking. However, ample room for improvement remains. Even the recent work of *Feng et al.* [2015], which employs a sophisticated watershed segmentation technique to identify individual cold pools, yields cold pool boundaries that in many cases take the form of straight lines rather than the arcs characteristic of outflow boundaries.

## **1.2 Goals**

The first goal of the research described in this thesis is to develop an objective algorithm for automated cold pool identification and tracking in numerical model outputs. The second goal is to use this objective algorithm to learn about how environmental characteristics influence cold pool development. In particular, this work will investigate the influence that soil moisture has on the development of cold pools in simulations of tropical continental convection.

## **1.3 Methods**

Throughout the thesis, the simulations analyzed are the sea-breeze simulations of *Grant and van den Heever* [2014]. All simulations were performed using the Regional Atmospheric Modeling System (RAMS) [*Cotton et al.*, 2003; *Saleeby and van den Heever*, 2013]. These simulations were performed in order to assess the separate and synergistic impacts of soil moisture, surface roughness length, and aerosols on tropical sea-breeze convection. The western third of the domain of these simulations is an ocean surface, and the eastern two-thirds are a land surface designed to emulate tropical rainforests. Although these simulations were designed to study sea-breeze convection, they also feature scattered daytime convection ahead of the sea breeze. It is the cold pools spawned by this convection that are analyzed in this thesis.

## **1.4 Thesis Structure**

Chapter 2 of this thesis addresses the first goal, i.e., to develop an objective algorithm for cold pool tracking. It begins with an overview of the terminology and methods that have been used to characterize and define convective cold pools in previous work. A detailed analysis is performed in order to assess which variables are best suited for defining edges of convective cold pools, and some of the shortfalls of existing methods are explored. Then, a novel approach to identifying and tracking convective cold pools is developed and tested on a simulation

containing many convective cold pools. This simulation is the control simulation of *Grant and van den Heever* [2014]. This approach identifies cold pool boundaries based on radial gradients in density potential temperature, and it is not only able to locate the boundaries of isolated convective cold pools, but it is also able to locate the boundaries between colliding cold pools in many situations. The algorithm is applied to an ensemble of convective cold pools, and the identified cold pools are averaged together to form a composite cold pool. The properties of the composite cold pool are then investigated. The results are largely consistent with previous studies of convective cold pools, helping to affirm the algorithm's validity. One new cold pool attribute that emerges from this analysis is what will be termed a *moist patch*. The moist patch is a region in which the ground has been soaked by rainwater, cooling the ground and locally delaying the recovery of near-surface temperatures to environmental values. This chapter is being prepared for submission to the *Journal of Advances in Modeling Earth Systems*.

Chapter 3 of this thesis addresses the second goal, i.e., applying the algorithm developed in Chapter 2 in order to learn about how soil moisture influences cold pool development. Three simulations, each initialized with different soil moisture content, are analyzed. These are the control simulation of *Grant and van den Heever* [2014] and the two simulations in which soil moisture is reduced. The algorithm developed in Chapter 2 is applied to each simulation to form three composite cold pools. Each composite cold pool is an average of the cold pools identified in a single simulation. Then, the composite cold pools are compared. The differences between the composite cold pools paint an interesting picture of how a simple variable like soil moisture can affect cold pool properties. It is found that the convective cold pools in the lowest-soil moisture simulation are stronger than those in the other simulations, with cooler temperatures relative to their surroundings and more vigorous associated circulations. It is further observed

that the structure of the cold pool water vapor field differs between simulations, which has implications for the organization of subsequent convection. This chapter is in preparation for submission to *Geophysical Research Letters*.

In summary, Chapter 2 explores the challenges of characterizing convective cold pools, presents a novel cold pool tracking algorithm, and analyzes the “average” cold pool that the tracking algorithm yields. Chapter 3 explores the effects of soil moisture on cold pool evolution. Finally, Chapter 4 summarizes the results of Chapters 2 and 3 and indicates some potential directions for future work.

## CHAPTER 2: CHARACTERIZING CONVECTIVE COLD POOLS

### 2.1 Introduction

A convective cold pool is a region of evaporatively cooled air that has been transported to the surface through convective downdrafts and has then, upon reaching the surface, spread out as a density current. Convective cold pools play an important role in multiple aspects of Earth's climate system, including the maintenance of long-lived squall lines [Rotunno *et al.*, 1988; Weisman and Rotunno, 2004] and the self-aggregation of tropical convection [Khairoutdinov and Randall, 2006; Jeevanjee and Romps, 2013b]. Despite the importance of convective cold pools, a consistent definition of these features has proved somewhat elusive. The lack of a common framework for describing convective cold pools may inhibit not only clarity of communication, but also clarity of thought. It is therefore useful to work toward a descriptive definition of convective cold pools and to clarify the meanings of various terms with related or overlapping definitions. Furthermore, the lack of a common framework for delineating cold pool boundaries may frustrate efforts to compare results between different studies. It is therefore useful also to work toward a practical definition of convective cold pools for data analysis. The primary goal of the present work is to help further this latter endeavor by reviewing the strengths and weaknesses of existing methods and then developing a novel method for defining convective cold pool boundaries.

We begin with an overview of the terminology used to describe convective cold pools. The American Meteorological Society (AMS) Glossary's definition for *cold pool* is as follows [American Meteorological Society, 2016a]:

1. (Also called cold drop, cold-air drop.) A region, or "pool," of relatively cold air surrounded by warmer air; the opposite of a warm pool.

This is usually applied to cold air of appreciable vertical extent that has been isolated in lower latitudes as part of the formation of a cut-off low. Cold pools are best identified as thickness minima on thickness charts. They are cyclonic-scale phenomena.

2. Any large-scale mass of cold air; a cold air mass or cold dome.

This definition captures some aspects of convective cold pools. For instance, convective cold pools are indeed “regions” of “relatively cold air surrounded by warmer air” [*American Meteorological Society*, 2016a]. Nevertheless, the definition appears not to have been drafted with convective cold pools—which are decidedly mesoscale rather than cyclonic-scale or large-scale—in mind.

Several terms have been used to describe convective cold pools and their attributes. Since the leading regions of cold pools have been shown to behave according to the physics of gravity currents [e.g., *Charba*, 1974], also known as density currents, these terms have also been used to refer to cold pools [e.g., *Grandpeix and Lafore*, 2010; *Wilbanks et al.*, 2015]. *Byers and Braham* [1949] primarily use the terms *cold dome* and *cold-air dome* but also use the terms *outflow* and *cold-air pool*. The term *cold dome* has received some continued use [e.g., *Caesar*, 1995; *Luo and Chen*, 2015] but has generally fallen out of favor. It should be noted that convective cold pools are not necessarily dome-shaped and in fact may exhibit their greatest depths near their leading edges as part of the “head” structure of the gust front [e.g., *Goff*, 1976; *Droegemeier and Wilhelmson*, 1987; *Wilbanks et al.*, 2015].

Other works, such as *Droegemeier and Wilhelmson* [1987], use the term *outflow*. One drawback of this term is that it takes on additional meanings in the context of convective systems, e.g., upper-level anvil outflows. Thus care must be taken with this term to ensure that the appropriate meaning is apparent in context.

Another term that has been used, particularly in studies of cold pools over tropical oceans, is *convective wake* [e.g., *Gaynor and Ropelewski, 1979; Nicholls and Johnson, 1984; Young et al., 1995; Geldmeier and Barnes, 1997; Qian et al., 1998*]. The term *wake* refers to regions within the boundary layer that have been modified by evaporatively cooled downdrafts. These regions remain part of the “wake” until they “recover” to pre-storm conditions. The term “wake” has drawbacks as well. The AMS Glossary defines “wake” as “the region of turbulence immediately to the rear of a solid body in motion relative to a fluid” [*American Meteorological Society, 2016b*]. The term “wake” connotes a rearward position when in fact a convective cold pool may propagate out ahead of its parent disturbance. It may be argued that a convective cold pool is a “wake” in that it is essentially the “aftermath” of a convective event. However, this meaning is not readily apparent. Another drawback is the relative lack of clarity in the literature as to what, precisely, constitutes a convective wake, i.e., whether the convective wake only includes the convective cold pool or whether it encompasses other phenomena as well.

Convective cold pools have also been described in terms of their edges. In conjunction with the term *outflow*, cold pool edges have been referred to as *outflow boundaries* [e.g., *Engerer et al., 2008*]. Other terms for the leading edge of a cold pool include *gust front* [e.g., *Wakimoto, 1982*], as well as, less commonly, *squall front* [*Zipser, 1977*] and *first gust* [*Byers and Braham, 1949*].

Just as there have been inconsistencies in the conceptual definition of convective cold pools, so too have there been inconsistencies in the practical definitions of convective cold pools used in data analysis. Often these definitions are specific to the particular data sets being examined. For instance, *Del Genio et al. [2012]* define cold pool grid boxes as grid boxes whose surface temperature is less than 31°C over land or less than 29°C over ocean. While such

thresholding yields satisfactory results in context, the thresholds themselves only apply to that particular study, and it becomes difficult to compare results across studies. Even criteria that do not rely on such simple thresholding may not be widely applicable. For instance, the convective cold pool detection algorithm of *Redl et al.* [2015] identifies convective cold pool events in time series data in part by requiring a 4 K increase in dew point temperature in a 30-minute time period. Although the approach yields satisfactory results over the dry regions of Northern Africa, the approach might not, as the authors note, succeed in higher-moisture environments in which cold pools may in fact be associated with sharp *decreases* in dew point temperature rather than increases.

One common approach for defining convective cold pools, especially in numerical model outputs, is to define cold pool air according to buoyancy, where buoyancy is defined, following *Tompkins* [2001] and *Emanuel* [1994], as:

$$B = g \frac{\theta_\rho - \bar{\theta}_\rho}{\bar{\theta}_\rho}, \quad (1)$$

where  $g$  is the acceleration due to gravity and  $\theta_\rho$  is the density potential temperature, defined as:

$$\theta_\rho = \theta \frac{1 + \frac{R_v}{R_d} r_v}{1 + r_v + r_{cond}} \approx \theta(1 + 0.608r_v - r_{cond}), \quad (2)$$

where  $\theta$  is the potential temperature,  $r_v$  is the mass mixing ratio of water vapor,  $r_{cond}$  is the mass mixing ratio of condensate, and  $R_v$  and  $R_d$  are the gas constants of water vapor and dry air, respectively. The overbar in  $\bar{\theta}_\rho$  in (1) denotes an “environmental” or reference value of density potential temperature, often derived from some horizontal average or taken to be the model base state value. In studies that define cold pools based on buoyancy, such as *Tompkins* [2001] and *Feng et al.* [2015], a buoyancy threshold is used such that all locations with buoyancy below the threshold are considered to be part of a cold pool. One limitation of this method of defining

buoyancy is that buoyancy is defined as a relative quantity. That is, a parcel’s buoyancy is determined by whether it is more or less dense than the “environmental” or reference value. However, as *Doswell and Markowski* [2004] explain, buoyancy is fundamentally not a relative quantity, and the choice of “environmental” or reference value is arbitrary. A buoyancy threshold used in one study may not be appropriate for use in a different study, and the results may not be directly comparable.

In the application of density current theory to convective cold pools, the formula for the theoretical density current propagation speed requires that the top height of the density current be specified. The formula for theoretical propagation speed  $C$  is as follows [*Rotunno et al.*, 1988]:

$$C^2 = -2 \int_0^h B dz, \quad (3)$$

where  $h$  is the top height of the cold pool. Again, the extent of the cold pool is often defined by setting some buoyancy threshold. In theory, the top of the cold pool should be defined as the height at which buoyancy first reaches zero, and the buoyancy should be calculated relative to the air ahead of the gust front. However, other choices are often made. For instance, *Feng et al.* [2015] use a buoyancy threshold of  $-0.003 \text{ m s}^{-2}$  to define the cold pool height, and buoyancy is calculated relative to a reference value derived from an average over both cold pool and non-cold pool points.

To the extent that modern cloud-resolving numerical models are able to simulate the evolution of convective cold pools, such models provide us with an opportunity to reassess our definitions of convective cold pools by examining the evolution of simulated cold pools across space and time within the full kinematic and thermodynamic model fields.

The structure of the remainder of this chapter is as follows: In Section 2.2, we review existing methods for defining convective cold pools and their boundaries in the analysis of

observational data and model outputs. The rest of this work relies on the analysis of a cloud-resolving model simulation; Section 2.3 introduces the model set-up. Then, in Section 2.4, we provide an overview of several model variables and assess their strengths and weaknesses for the purpose of delineating convective cold pool boundaries. The insights gained from this investigation help to guide the development of a new cold pool identification and tracking algorithm, which is introduced in Section 2.5. The algorithm described in Section 2.5 is applied to the simulation described in Section 2.3, and the identified cold pools are averaged together to create a composite cold pool. The properties of the composite cold pool are explored in Section 2.6. The cold pool identification algorithm only identifies cold pools at the lowest model level; Section 2.7 explores some of the challenges associated with identifying convective cold pools in three dimensions. Finally, Section 2.8 concludes the paper.

## **2.2 Defining Cold Pools for Data Analysis**

In observational studies and in modeling studies, various methods have been developed to analyze various aspects of convective cold pools. Some methods aim to identify entire cold pools; other methods seek only to identify particular attributes such as cold pool depth or particular events such as gust front passage. This section reviews the methods that various studies—first observational studies, then modeling studies—have used.

Convective cold pools are spawned by precipitating clouds. Thus, perhaps the simplest metric for defining convective cold pools is the onset of precipitation. *Young et al.* [1995], in their analysis of data from the Tropical Ocean Global Atmosphere Coupled Ocean-Atmosphere Response Experiment (TOGA-COARE), defined the arrival of convective cold pools according to the onset of precipitation with a rate of at least  $2 \text{ mm h}^{-1}$ , a threshold shown by *Barnes and Garstang* [1982] to be indicative of precipitation that is accompanied by downdrafts originating

from above the subcloud layer. In their analysis of data from the Rain in Cumulus over the Ocean (RICO) experiment, *Zuidema et al.* [2012] used a similar method for defining cold pool onset but instead used a threshold of  $0 \text{ mm h}^{-1}$ .

Another metric for defining convective cold pools is temperature  $T$ . Air with low temperature or potential temperature relative to its surroundings is defined to be cold pool air. In an analysis of data collected during the GARP Atlantic Tropical Experiment (GATE), *Gaynor and Ropelewski* [1979] used a combination of shipborne acoustic sounder data and subjective inspection of the 10-m dry-bulb temperature measurement to classify the state of the boundary layer into three categories: 1) *undisturbed*, 2) *early perturbed or density current*, and 3) *mature perturbed or wake*. Temperature decreases were used to determine the onset of density current conditions, i.e., the passage of the gust front, as well as the duration of the latter two categories. *Barnes and Garstang* [1982] used thresholds of  $\frac{dT}{dt}$  to classify conditions into similar categories: 1) *undisturbed*, 2) *convectively active*, and 3) *wake*. *Young et al.* [1995], too, looked at temporal trends in air temperature to determine the recovery of the boundary layer following the onset of a cold pool. In particular, the boundary layer was defined to have finished recovering from the initial drop in temperature either when the temperature had increased to the value of the sea-surface temperature (SST) or when the temperature had stopped increasing and begun to decrease again. In another analysis of TOGA-COARE data by *Saxen and Rutledge* [1998], the onset of the cold pool was defined according to an initial temperature decrease of at least 1 K. Both *Saxen and Rutledge* [1998] and *Zuidema et al.* [2012] define recovery using similar methods to *Young et al.* [1995]. As in *Gaynor and Ropelewski* [1979], *Barnes and Garstang* [1982], and *Saxen and Rutledge* [1998], it has become common to define the onset or boundary of the cold pool according to some drop in temperature or potential temperature. *Terai and Wood*

[2013] use such an approach in their analysis of aircraft observations of marine stratocumulus-generated cold pools, as do *Yokoi et al.* [2014], *Feng et al.* [2015], and *Provod et al.* [2016] in their analyses of time series data.

A somewhat more appropriate metric for defining convective cold pools is density. Cold pools have been shown to act as density currents [e.g., *Charba*, 1974], and their behavior is thus dictated in part by the difference in density between cold pool air and that of the ambient air. A related metric is buoyancy  $B$ , which is calculated according to the deviation in density between a parcel and some base state. Other related metrics include virtual (potential) temperature and density (potential) temperature, in which corrections are applied to the (potential) temperature field to account for the effects of water vapor, as well as, in the case of density (potential) temperature, hydrometeor loading, on parcel density. The use of density and related variables mirrors that of temperature. *Addis et al.* [1984] defined gust front occurrence as a 0.5 K decrease in virtual temperature over approximately 3 minutes in time series data, and *Wilbanks et al.* [2015] defined density current occurrence as a  $1 \text{ g m}^{-3}$  density increase over a distance of 3.5 km.

Various aspects of the wind field have also been used to define convective cold pools. Convective cold pools are characterized by surface divergence in the center of the cold pool where downdraft air spreads out, as well as by surface convergence at the leading edge of the cold pool. Thus, *Uyeda and Zrnić* [1986] identified gust fronts by looking for a convergence line in the Doppler velocity field. More recently, *Kilpatrick and Xie* [2015] identified convective cold pools in scatterometer data by looking for a local maximum in the surface wind divergence. The leading edge of the cold pool, also known as the *gust front*, is characterized not only by convergence but also by locally stronger winds whose direction may differ from that of the

environmental flow. *Engerer et al.* [2008] identified convective cold pools according to a sharp shift in wind direction in time series data. Building on this work, *Provod et al.* [2016] defined cold pools primarily based on a wind shift. Furthermore, *Redl et al.* [2015] and *Provod et al.* [2016] both included an increase in horizontal wind speed among their criteria for detecting convective cold pool passage. One limitation of identifying cold pool arrival based on wind shift is that some locations may not experience a wind shift; in these cases, the cold pool will not be detected.

Another metric that has been used to identify the arrival of cold pools is the dew point temperature, used by *Redl et al.* [2015] in relatively dry regions of northern Africa. In particular, the algorithm of *Redl et al.* [2015] looks for sudden increases in dew point temperature. As discussed in the introduction, one limitation of this approach is that in moister regions, convective cold pools may be characterized by sudden *decreases* in dew point temperature, not increases.

Not discussed above are attempts to define the tops of cold pools, or cold pool depths, in observational data. As discussed in the introduction, cold pool depth must be determined in order to calculate the theoretical density current propagation speed. One method for estimating cold pool depth, used by *Terai and Wood* [2013], is to measure the pressure and density inside and outside the cold pool, and then to use the hydrostatic equation to determine the cold pool depth. This method, however, assumes a constant density perturbation throughout the depth of the cold pool. Another method, used by *Wilbanks et al.* [2015], is to examine the Doppler velocity field and to define the cold pool top as the level at which speed shear near the surface gives way to directional shear aloft. A third method, used by *Bryan and Parker* [2010], is based on buoyancy: a “cold pool” sounding is compared to an “environmental” sounding, and the depth of the cold

pool is determined to be the level at which the buoyancy first reaches  $0 \text{ m s}^{-2}$ , i.e., the virtual potential temperature of the cold pool sounding ceases to be less than the that of the environmental sounding. One limitation of this method is that the depth of the cold pool may depend substantially upon the choice of reference sounding. For example, the cold pool analyzed by *Bryan and Parker* [2010] had a depth of either 3.6 km or 4.0 km depending on which of two reference soundings was used.

Modeling studies have fewer observational constraints than do observational studies because the state of the entire model domain, in terms of a wide array of variables, can be known at any given time during a simulation. Thus, it is possible to take a more comprehensive approach to defining cold pools. Rather than defining a single point in time series data at which the gust front arrives, the boundaries of the entire cold pool may be delineated.

In modeling studies, cold pools are often defined as regions that satisfy some threshold in temperature or some other thermodynamic variable. In *Tompkins* [2001], cold pool air was defined as air whose buoyancy is less than  $-0.005 \text{ m s}^{-2}$ , where buoyancy is defined relative to the horizontal domain mean value. The same approach was used in *Seigel* [2014]. *Feng et al.* [2015] also used this approach, albeit with a threshold of  $-0.003 \text{ m s}^{-2}$  and with buoyancy defined relative to a locally computed horizontal average rather than a full-domain average. *Feng et al.* [2015] then applied a watershed segmentation algorithm to separate regions satisfying this threshold into individual cold pools. *Feng et al.* [2015] used the same threshold to define the cold pool depth for the calculation of the theoretical density current propagation speed. *Seigel and van den Heever* [2013] and *Seigel et al.* [2013] used a threshold of  $-0.05 \text{ m s}^{-2}$  for the same purpose. *Torri et al.* [2015] used perturbation density potential temperature  $\theta_\rho'$ , a variable related to buoyancy, to define cold pool parcels. Specifically, a threshold of  $-1 \text{ K}$  was used. Additional

variables related to buoyancy, such as perturbation virtual potential temperature  $\theta_v'$  and virtual temperature  $T_v$ , have also been used to define convective cold pools. *Li et al.* [2014] used a combination of  $\theta_v'$ , wind speed, and precipitation to define cold pool boundaries. *Gentine et al.* [2016] applied a k-means image segmentation algorithm to the  $T_v$  field to determine cold pool pixels.

Temperature has also been used to define convective cold pools in modeling studies. As discussed in the introduction, *Del Genio et al.* [2012] defined cold pool grid boxes using thresholds in temperature. In a study by *Sato et al.* [2009], cold pool formation events were defined as drops in temperature of at least 1.5 K in a 1.5-h period.

Several modeling studies have used the perturbation equivalent potential temperature,  $\theta_e'$ , to define convective cold pools. *Dawson et al.* [2010] defined cold pool grid boxes using a threshold of  $\theta_e' \leq -1$  K. *Katona et al.* [2014] used the same threshold alongside a simulated reflectivity threshold to ensure the presence of rain. *Schlemmer and Hohenegger* [2014] defined cold pools using a threshold of  $\theta_e' \leq -2$  K averaged over the lowest  $\sim 500$  m of the domain.

As mentioned above, *Li et al.* [2014] included model wind speed as part of their algorithm for determining cold pool boundaries. *Langhans and Romps* [2015] also used model winds to determine cold pool boundaries. In particular, the radius of the cold pool at each azimuth angle was defined as the maximum radius at which the vertical motion exceeded some threshold value.

### **2.3 Model Setup**

This study analyzes cold pools within the control simulation of *Grant and van den Heever* [2014]. The simulation was run using the open-source Regional Atmospheric Modeling System (RAMS) (<http://reef.atmos.colostate.edu/~sue/vdhpage/rams.php>) [*Cotton et al.*, 2003;

*Saleeby and van den Heever, 2013*], coupled to the Land-Ecosystem-Atmosphere-Feedback (LEAF) version 3 land surface model [*Walko et al., 2000*].

The model configuration is summarized in Table 2.1. The simulation was designed for the study of tropical sea-breeze convection. Thus, the domain was non-rotating ( $f=0$ ), and the western one-third of the domain had an ocean-type surface, whereas the eastern two-thirds of the domain had a tropical rainforest-type surface. The simulation was initialized at 600 UTC (700 LT) and run for 16 hours in order to capture the development of the sea breeze and convection over the course of the day. The size of the domain was 200 km (meridional)  $\times$  550 km (zonal)  $\times$  26 km (vertical), and the simulation was run with a horizontal grid spacing of 1 km, and 57 stretched vertical levels with 100 m grid spacing near the surface increasing to 1 km aloft.

Figure 2.1 shows a snapshot of density potential temperature,  $\theta_\rho$ , at the lowest model level. Values of  $\theta_\rho$  are lowest within the oceanic part of the domain and within the sea breeze. Ahead (to the east) of the sea breeze are dozens of convective cold pools at various stages of their life cycles. The present study focuses on the convection that develops ahead of the sea breeze and the cold pools produced by this convection. The sea-breeze identification method of *Grant and van den Heever [2014]* is used to locate the sea-breeze front, and only cold pools forming ahead of the sea-breeze front and more than 50 km from the eastern edge of the domain are analyzed. In the sections that follow, several perturbation quantities are discussed and shown. As in *Grant and van den Heever [2014]*, these are defined relative to an average over the part of the domain that extends from 10 km ahead of the identified sea-breeze front location to 50 km from the eastern edge of the domain.

## 2.4 Choice of Variables

The preceding discussion identifies several variables that have been used to define convective cold pool boundaries and attributes in previous work. In this section we examine several such variables, along with a few additional ones, and assess each variable's utility for characterizing convective cold pools according to the following criteria:

(i) There should exist some physical basis for using this variable to define convective cold pools.

(ii) When this variable is plotted, cold pool edges should be apparent and in the correct locations. It should be possible to distinguish cold pools that collide with one another.

(iii) It should be possible to locate cold pool edges without the use of arbitrary thresholds. If thresholds must be used, then they should have some physical basis, and the resulting edges should be relatively insensitive to the choice of threshold.

It will be shown that although several variables satisfy some of these criteria, none satisfy all of these criteria. In the discussion that follows, a single, illustrative convective cold pool is examined in terms of several different variables. The evolution of this cold pool is shown in Figure 2.2. This specific cold pool is particularly “well-behaved” in that it is isolated, approximately circular, and creates robust perturbations to various dynamic and thermodynamic fields. For this reason, its boundaries should be particularly easy to define. Although only a single cold pool is shown, the conclusions that it yields regarding the different variables are representative of the other cold pools in the simulation. For some variables, this cold pool is shown at multiple times; the time used most often will be defined as  $t = 0$ , and other times will be defined relative to this first time. We now consider the strengths and weaknesses of ten potentially useful variables to identify cold pools.

### 2.4.1 Buoyancy

As is noted in *Tompkins* [2001], buoyancy  $B$  is a natural choice for defining convective cold pools since cold pools act as density currents. Thus there is a strong physical basis for using buoyancy, as well as related variables such as density potential temperature  $\theta_\rho$ , to define cold pool boundaries. As Figure 2.3 shows, the buoyancy field also exhibits sharp gradients at the boundary of the cold pool as negative buoyancy inside the cold pool gives way to positive buoyancy outside the cold pool. These gradients necessarily occur at the edge of the density current. There therefore exists a physical basis for stating that these gradients, as well as any edges derived using these gradients, are in the “correct” location. In the discussion that follows, the “correct” location of the cold pool boundary will be taken to be the location of the gradient in the buoyancy field.

Despite the strengths of the buoyancy field, there are some drawbacks. One drawback is that for any choice of buoyancy threshold, the size of the cold pool eventually begins to decrease with time as the cold pool dissipates and regions of negative buoyancy disappear, as is shown in Figure 2.3. If we consider the boundary to be the location of the gust front, then a decrease in cold pool area would correspond to a retreat of the gust front. Under this interpretation of the boundary of a cold pool, this is not a physical outcome; gust fronts propagate outward from the center of the cold pool and do not normally retreat. Another drawback lies in the choice of threshold. As discussed in the introduction, the definition of buoyancy relies on the specification of an arbitrary reference state. For this reason, there is no physical basis for any particular choice of buoyancy threshold.

Figure 2.4 shows several scenes that feature colliding cold pools. It is apparent that a simple buoyancy threshold will not suffice to identify the edges of the various cold pools.

However, from these scenes it does seem possible to discern the locations of the cold pool boundaries by visual inspection (assuming some knowledge on the part of the viewer). Thus we can state that the buoyancy field does contain information about where the boundaries are. Analysis methods more sophisticated than the application of a uniform threshold may be able to identify the boundaries of colliding cold pools based on the information present in the buoyancy field. Indeed, *Feng et al.* [2015] achieved some success applying a watershed segmentation technique to the buoyancy field. The method developed in Section 2.5 of the present work is able to discern the boundaries of colliding cold pools using the density potential temperature field, which is identical in structure to the buoyancy field.

#### 2.4.2 *Water Vapor Mixing Ratio*

In the simulation examined here, convective cold pools are characterized by a ring of enhanced moisture along the periphery of the cold pool surrounding a relatively dry cold pool interior, as is shown in Figure 2.5b. This structure, however, may be different in other environments. In fact, the time series of dew point temperature in *Redl et al.* [2015, their Figure 3c] for cold pools in northwest Africa do not suggest the presence of a dry cold pool interior and instead suggest that cold pool air in such regions may, in fact, be relatively moist throughout. As pointed out in *Langhans and Romps* [2015], rings of enhanced moisture occur in large part due to surface latent heat fluxes, which themselves depend on surface properties. Furthermore, an arbitrary threshold would be necessary in order to use water vapor mixing ratio to determine convective cold pool boundaries. For these reasons, water vapor mixing ratio is ill suited for this task.

### *2.4.3 Equivalent Potential Temperature*

Although equivalent potential temperature  $\theta_e$  has many attractive qualities, such as its conservation under moist pseudoadiabatic processes, there is limited physical basis for using it to define convective cold pool boundaries. In fact, the boundaries that might be obtained using  $\theta_e$  do not necessarily match those that would be obtained using buoyancy or  $\theta_p$ . This is due to the role that water vapor has in the calculation of  $\theta_e$ . As discussed in Section 2.4.2, the simulation examined here exhibits rings of enhanced water vapor at the periphery of convective cold pools. These rings of enhanced water vapor, which occur in regions of negatively buoyant air, raise the local values of  $\theta_e$  along cold pool peripheries such that cold pools appear to be smaller in the  $\theta_e$  field than in the  $\theta_p$  field, as can be seen in Figure 2.5c. If, as discussed in Section 2.4.1, the buoyancy-derived boundaries are taken to be the correct boundaries, then this means that cold pools identified based on the  $\theta_e$  field may be too small, and caution should be used when using  $\theta_e$  to define convective cold pool boundaries.

### *2.4.4 Perturbation Pressure*

There does exist a physical basis for defining convective cold pools based on perturbation pressure. Cold pools act as density currents, and by the hydrostatic relation, the increased density associated with convective cold pools should be accompanied by a positive pressure perturbation. However, the warm air aloft associated with cold pools' parent cloud systems creates a negative pressure perturbation, which can cancel out some of the positive pressure perturbation associated with the cold pool. Furthermore, as Figure 2.5d shows, the perturbation pressure field does not exhibit any clear edges (i.e., no sharp gradients). Thus, the perturbation field is not well suited for determining convective cold pool boundaries.

#### 2.4.5 Static Stability

When downdraft air reaches the ground, it spreads out, coating the surface with cool air to form a cold pool. This air has a lower potential temperature than the air above it, and thus there exists a layer of stable stratification. This is the physical basis for using static stability,  $\frac{\partial\theta}{\partial z}$ , to define convective cold pools. A potential threshold for defining the boundary of convective cold pools is  $\frac{\partial\theta}{\partial z} = 0$ ; this threshold has some physical significance as the threshold for absolute static stability. As Figure 2.6 shows, the static stability field does exhibit large gradients. However, these gradients do not necessarily occur in the “correct location” discussed in Section 2.4.1; the turbulence associated with the cold pool gust front may prevent stable stratification along the periphery of the cold pool. Furthermore, as was the case with the buoyancy field, the cold pool area defined by a given static stability threshold tends to decrease as the cold pool dissipates; this result is unphysical for reasons discussed in Section 2.4.1. Finally, the usefulness of static stability for defining convective cold pool boundaries may depend on model grid spacing near the surface, as well as the particular situation, e.g., whether the ambient air is already stably stratified. For these reasons, we hesitate to use static stability to define convective cold pool boundaries.

#### 2.4.6 Radial Velocity

As downdraft air reaches the surface, it spreads out, forming a density current propagating in the radially outward direction. Thus, there is a strong physical basis for defining convective cold pools according to the radial velocity field. Indeed, the terms *outflow* and *gust front*, discussed in the introduction, both refer to radially outward winds. Furthermore, as Figure 2.7d shows, the radial velocity field exhibits a strong radial gradient as the strong radial winds of the gust front give way to the weaker ambient flows outside the cold pool. There are additional

potential advantages of using the radial velocity  $v_r$  to define convective cold pool boundaries. One potential advantage is that there exists a physically based threshold of  $0 \text{ m s}^{-1}$  that might be used to delineate cold pool boundaries. Another potential advantage is that the boundaries between colliding cold pools become immediately apparent in the  $v_r$  field: from the perspective of some given cold pool, the radial outflow associated with an adjacent cold pool will be directed radially inward. The boundary between the given cold pool and the adjacent one would simply be the zero contour of  $v_r$ .

In practice, unfortunately,  $v_r$  does not live up to its promise. Even though a physically based threshold exists, it only works when the ambient flows are directed radially inward. Moreover, the raw  $v_r$  field does not yield discrete boundaries between colliding cold pools (Figure 2.8). Attempts to identify boundaries between colliding cold pools using the more sophisticated methods of Section 2.5 with  $v_r$ , while successful, appear generally to be no more successful than attempts based on buoyancy or  $\theta_\rho$  (not shown). There exist other drawbacks as well. One is that a cold pool center must be specified in order to calculate the radial component of the wind. Another is that boundaries obtained using  $v_r$  are not quite in the “correct location” established in Section 2.4.1. As shown in Figures 2.7c-d, the region of enhanced  $\frac{\partial v_r}{\partial r}$  lies radially outside the region of enhanced  $\frac{\partial \theta_\rho}{\partial r}$ . This result is typical of convective cold pools in this simulation. Thus, cold pools identified using  $v_r$  will be larger than those identified using buoyancy or  $\theta_\rho$ .

#### 2.4.7 Vertical Velocity

Convective cold pools are spawned by downdrafts, and along cold pool edges, convergence of the horizontal wind field yields rising motion. The latter motion is referred to by Goff [1976] as the *prefrontal updraft*. Thus there does exist a physical basis for defining cold

pool boundaries in terms of vertical velocity. There is a transition from downdrafts inside the cold pool to updrafts outside the cold pool; this transition serves as physical justification for a vertical velocity threshold of  $0 \text{ m s}^{-1}$ . Furthermore, there are strong gradients in vertical velocity associated with this transition. These gradients are located in approximately the same location as the gradients in buoyancy and are thus in the “correct location” discussed in Section 2.4.1 (Figures 2.7e-f). However, the signature ring of downdrafts surrounded by updrafts only exists in areas and during times in which the cold pool is actively expanding. Factors such as turbulence may interfere with this signature pattern as well. In an examination of the near-surface vertical velocity field for many convective cold pools within the simulation (not shown), it is often the case that the zero contour in vertical velocity does not completely circumscribe the cold pool; there is no closed contour. Based on this result, we have concluded that vertical velocity is not the best option for identifying convective cold pool boundaries.

#### *2.4.8 Surface Latent Heat Flux*

In *Tompkins* [2001], convective cold pools are observed to be collocated with large enhancements in the surface latent heat flux. It is therefore worth exploring whether surface latent heat fluxes can be used to define convective cold pool boundaries. In the idealized simulation of *Tompkins* [2001], there are two factors that allow enhanced surface latent heat fluxes in convective cold pools: the relatively dry cold pool interior (see Section 2.4.2), into which enhanced evaporation may occur, and the strong winds associated with the cold pool outflow (see Section 2.4.6). In the simulation examined in the present work, we do not observe enhanced latent heat fluxes throughout the convective cold pools; in fact, the interiors exhibit markedly decreased latent heat fluxes (Figure 2.9a). These regions of decreased latent heat fluxes are due in part to relatively calm winds near the center of the cold pool, as well as in part to the

enhanced relative humidity (which itself is due to cool temperatures rather than enhanced mixing ratios). However, the major player in suppressing latent heat fluxes near the center of the cold pool appears to be shading of shortwave radiation by the cold pool's parent cloud system (Figure 2.9b). In regions that are shaded, there is less incoming energy available with which to perform evapotranspiration, and thus latent heat fluxes. Unlike the simulation of *Tompkins* [2001], the simulation analyzed in the present work uses an interactive radiation scheme, and so the effects of shading can be realized. The heterogeneities in the surface latent heat flux field, as well as the lack of a physically meaningful threshold value, render it ill suited for determining convective cold pool boundaries.

#### 2.4.9 Surface Sensible Heat Flux

It is noted in *Tompkins* [2001] that the boundary-layer temperatures and surface sensible heat fluxes are “almost perfectly negatively correlated.” *Tompkins* [2001] uses a fixed-sea surface temperature (SST) surface. Where boundary-layer temperatures much lower than the SST, there is a larger temperature differential, and thus surface sensible heat fluxes are enhanced. Surface sensible heat fluxes are enhanced further by the presence of gusty cold pool winds. Thus there appears to be a physical basis for defining convective cold pools in terms of the surface sensible heat fluxes. However, in the simulation analyzed in the present work, there is an interactive surface model. Therefore, the patterns in the sensible heat flux field are potentially more realistic. Although there are strong gradients in the surface sensible heat flux field (Figure 2.9c), these gradients are associated not with the temperature gradients of the cold pool, but rather with regions in which precipitation has soaked the ground, thereby lowering the surface temperature. Thus, the edges are not in the “correct location” established in Section 2.4.1, and

surface sensible heat flux is not a suitable variable for determining convective cold pool boundaries.

#### *2.4.10 Density Potential Temperature Advection*

One field that has received less attention in the literature is the horizontal density potential temperature advection,  $-\vec{v}_H \cdot \vec{\nabla}_H \theta_\rho$ , which is displayed in Figure 2.9d. This field shows where cool air is advected into warmer regions as the cold pool spreads out. Thus, this field illustrates the active edge of the cold pool. There is a ring of strong negative values around the periphery of the cold pool, where cooler air is arriving. There is thus a strong physical basis for using this field to define convective cold pools, and it can be used to determine boundaries that are in the “correct location.” One drawback to using this field is that an arbitrary threshold must be applied. The field is almost uniformly negative, and so a physically based threshold of  $0 \text{ K s}^{-1}$  will not work. Nevertheless, if one is willing to apply an arbitrary threshold, then this could prove to be a useful field for identifying convective cold pool boundaries.

### **2.5 Algorithm for Cold Pool Identification and Tracking**

#### *2.5.1 Algorithm Development*

The use of spatial derivatives can allow us to minimize the use of arbitrary thresholds. When spatial derivatives are used, there is inherent physical meaning in a threshold of zero. Where the first derivative equals zero, there is a peak or a trough. Where the second derivative equals zero, there is an inflection point.

The spatial derivatives of several variables were assessed to see whether the zero-contours of their first and second derivatives yielded reasonable cold pool boundaries. The best results, as assessed subjectively, were obtained using the zero-contour of the second radial derivative of density potential temperature,  $\frac{\partial^2 \theta_\rho}{\partial r^2}$ . Figures 2.10 and 2.11 illustrate why this

approach yields suitable results. Consider an idealized circular, axisymmetric cold pool in which the inside of the cold pool has a uniform cool temperature and the environment has a uniform warmer temperature, as shown in Figure 2.10. The inflection point of the  $\theta_\rho(r)$  curve in Figure 10a, which is also the point at which  $\frac{\partial^2\theta_\rho}{\partial r^2} = 0$  in Figure 2.10c, appears subjectively to be a suitable choice of cold pool boundary. This reasoning extends to non-idealized, non-axisymmetric cold pools as well, provided that their shapes are nearly circular.

Figure 2.11 illustrates this approach for the cold pool examined in Section 2.4. Figure 2.11a shows the  $\theta_\rho$  field. As discussed previously, the cold pool is characterized by a region of low  $\theta_\rho$  approximately 5 km in radius. One might imagine a radial  $\theta_\rho$  profile like that in Figure 2.10a, with low values of  $\theta_\rho$  near the center transitioning to higher values of  $\theta_\rho$  outside of the cold pool. The center of the cold pool is determined according to a method described later in this section, and the first and second radial derivatives,  $\frac{\partial\theta_\rho}{\partial r}$  and  $\frac{\partial^2\theta_\rho}{\partial r^2}$ , are shown in Figures 2.11b and 2.11c, respectively. Figure 2.11b shows an annular region of enhanced  $\frac{\partial\theta_\rho}{\partial r}$  values, that is, enhanced radial gradient in  $\theta_\rho$ , surrounding the cold pool. This corresponds to the idealized peak shown in Figure 2.10b. Figure 2.11c depicts a region of positive  $\frac{\partial^2\theta_\rho}{\partial r^2}$  values surrounded by negative  $\frac{\partial^2\theta_\rho}{\partial r^2}$  values. These correspond to the positive and negative lobes in Figure 2.10c. The zero-crossing of the curve in Figure 2.10c corresponds to the zero-contour of Figure 2.11c. This zero-contour is then taken to be the boundary of the cold pool. When this boundary is superposed onto the original  $\theta_\rho$  field in Figure 2.11a, the result is a snug fit to the regions in which  $\theta_\rho$  has the strongest gradients. When this boundary is superposed onto the vertical velocity field, as in Figure 2.12d, we find that the boundary closely follows the zero-contour of vertical velocity, i.e.,

the location at which near-surface downdrafts near the center of the cold pool give way to near-surface updrafts at the periphery of the cold pool. The closeness of the zero-contour of vertical velocity to the cold pool boundary obtained using this method is not unique to this particular cold pool and is in fact typical of the cold pools in the simulation, as will be shown.

The question then arises, Why not simply use the zero-contour of vertical velocity in order to define cold pool edges rather than go through the trouble of calculating the second radial derivative of  $\theta_\rho$ ? Several variables were tested in order to address this question; some additional examples are shown in Figure 2.12. It was determined that  $\frac{\partial^2 \theta_\rho}{\partial r^2}$  most reliably yielded closed contours in subjectively reasonable locations. Compared to vertical velocity (Figure 2.12b), which performs well in the example shown, it was found that  $\frac{\partial^2 \theta_\rho}{\partial r^2}$  yielded closed contours earlier in the cold pool lifecycle. One alternative to using the second radial derivative of  $\theta_\rho$  is to use the horizontal Laplacian of  $\theta_\rho$  (Figure 2.12d). These two options are similar in formulation, and in the presence of axisymmetry, the horizontal Laplacian simplifies to the second radial derivative. One advantage of the horizontal Laplacian is that it can be calculated without first determining a cold pool center. However, it is observed that the horizontal Laplacian does not yield clean, closed contours surrounding cold pools, as is the case in the case shown (compare Figure 2.11c to Figure 2.12d).

The specific procedure by which cold pools are identified will now be described. Before we can calculate the second radial derivative of the  $\theta_\rho$  field, we must first identify a cold pool center. Before we can identify a cold pool center, we must first identify areas of interest where cold pools are likely to be located. Since cold pools are spawned by precipitating clouds, we first identify areas of interest based on the surface rainfall rate. Specifically, areas of interest are

defined as contiguous regions in which the surface rainfall rate exceeds some threshold value. Each area of interest corresponds to one potential cold pool. Unfortunately, an arbitrary threshold rainfall rate must be chosen here. A threshold of  $1 \text{ mm h}^{-1}$  is used. This threshold is somewhat more permissive than the  $2 \text{ mm h}^{-1}$  threshold for penetrating downdrafts determined by *Barnes and Garstang* [1982] and used by *Young et al.* [1995], but it is of the same order of magnitude. Areas of interest are contiguous regions where the surface rainfall rate meets or exceeds the  $1 \text{ mm h}^{-1}$  threshold, where pixels are defined as contiguous if they share an edge, but not if they only share a corner (i.e., 4-connectivity). For purposes of this processing step, any “holes”, i.e., pixels below the  $1 \text{ mm h}^{-1}$  threshold embedded within a region of pixels meeting or exceeding the threshold, are filled in. Then, any regions of area less than  $8 \text{ km}^2$  (8 square-kilometer pixels) are discarded in order to ensure that only robust rainy regions are selected. The centroid of each region is then calculated.

The centroid of each region of contiguous rainy pixels is taken to be the center of a possible cold pool. There is typically some delay between the appearance of a rainy region and the emergence of the cold pool it spawns, at least within the near-surface  $\theta_\rho$  field. Therefore, the next step of the cold pool identification process is applied to the thermodynamic fields 10 minutes following the identification of the respective rainy regions.

In the next step, convective cold pool boundaries are located as described above using the second radial derivative of density potential temperature,  $\frac{\partial^2 \theta_\rho}{\partial r^2}$ , where the radial coordinate is defined with respect to the centroid of the corresponding rainy region. First, each rainy region’s centroid is computed, and the radial derivatives of  $\theta_\rho$  are calculated accordingly. Then, contiguous regions are identified in which  $\frac{\partial^2 \theta_\rho}{\partial r^2} > 0$ , and any “holes” in these regions are filled

in. The boundary of the cold pool may be chosen from the boundaries of these regions. A region's boundary will be chosen if the boundary meets the following criteria:

1. If there are multiple regions, then this region's centroid is closest to that of the original rainy region. Furthermore, the distance between this region's centroid and that of the original rainy region must be less than or equal to the equivalent diameter of the original rainy region, where the equivalent diameter is defined as the diameter of a circle whose area equals that of the original rainy region.
2. This region must occupy at least 90% of the original rainy region's pixels, and the original rainy region (which is typically smaller) must occupy at least 25% of the region's pixels.
3. The region must be approximately circular: The region's aspect ratio (the ratio of its minor axis to its major axis) must be greater than or equal to 0.7, and its solidity (the ratio of the object's area to that of its convex hull) must be greater than or equal to 0.8.

If no contiguous region meets all of the above criteria, then the boundary remains undefined, and the original rainy region is discarded. If a region does meet all of the above criteria, then its boundary is taken to be the boundary of the cold pool, and its centroid is taken to be the centroid of the cold pool for all further calculations.

Cold pools are identified at each output time independently of other output times. However, the tracking of cold pools over time is a powerful tool that can be used to probe the cold pool life cycle. Thus, after this identification step, cold pools are tracked between successive output times. Each cold pool at output time  $t$  is compared to the cold pools at output time  $t + 1$ . In order to find a match between the cold pool at time  $t$  and one of the candidate cold pools at time  $t + 1$ , the following criteria must be met:

1. If there are multiple candidate cold pools at time  $t + 1$ , then this candidate cold pool's centroid must be closest to that of the original cold pool at time  $t$ . Furthermore, the distance between the centroids must be no larger than the equivalent radius (the radius of a circle of equivalent area) of the original cold pool at time  $t$ .
2. This cold pool must occupy at least 50% of the original cold pool's pixels, and vice-versa.

For the purposes of the present work, the tracking of cold pools over time is only used to prevent the overrepresentation of particular cold pools within the data used to generate statistics about cold pool attributes. Tracking provides information regarding how many times a particular cold pool has been identified. The analyses that follow use the information that is collected at the *first* output time at which each cold pool is identified.

Composites are constructed so as to capture the “average” structure and evolution of cold pools. In order for composites to be constructed, cold pools must be “aligned” in time and space. Cold pools are aligned in time according to the first output time at which each cold pool is identified by the cold pool identification algorithm. They are aligned in space according to their centroids. Data are then interpolated onto a cylindrical polar grid with dimensions of  $\Delta r = 1$  km and  $\Delta\phi = \frac{2\pi}{180}$  rad. Radial profiles are then constructed for each cold pool at each height by averaging the interpolated data across  $\phi$ . Composites may then be constructed for any set of cold pools by averaging the radial profiles.

These composites, when constructed for a variety of variables, capture the mean structure of an ensemble of cold pools. If it is further assumed that cold pools are approximately stationary, then the mean evolution can also be captured by projecting cold pool centroids forward and backward across output times (e.g., to 15 minutes after each cold pool was first

identified) and constructing composites at those times according to the same procedure. It is assumed that the centroid remains stationary over time. This compositing approach is similar to that of Tompkins (2001), which also constructed composite radial profiles, albeit based upon “handpicked” cold pools rather than objectively identified ones.

### 2.5.2 Algorithm Performance

Figure 2.13 shows the algorithm performance for an array of convective cold pools from within the simulation described in Section 2.3. For a variety of convective cold pool strengths and shapes, the algorithm yields subjectively reasonable boundaries that align with the gradients in  $\theta_\rho$ . Figure 2.14 shows the performance of the algorithm for the scenes of colliding cold pools discussed in Section 2.4. The algorithm is able to find suitable boundaries for all of the scenes of colliding cold pools shown. This is not always the case. For example, Figure 2.15 shows a case in which a new cold pool forms along the periphery of an existing cold pool. In this case, the new disturbance ends up as part of the existing disturbance when the  $\frac{\partial^2 \theta_\rho}{\partial r^2} = 0$  contour is plotted. The algorithm has other limitations; these are discussed in Section 2.8.

## 2.6 Composite Cold Pools

### 2.6.1 Overview

Figures 2.16 and 2.17 show composites of surface and near-surface quantities over time, from 30 minutes before each cold pool is identified until 120 minutes after each cold pool is identified, in 15-minute increments. The composites were constructed using the 138 cold pools identified from 14:15 to 15:15 LT within the simulation described in Section 2.3. These composites are plotted relative to the convective cold pool centroid ( $r = 0$  km), henceforth referred to as the *center*. It should be noted that these composites capture a combination of cold pool evolution and the diurnal cycle. In order to help distinguish between the effects of cold pool

evolution and those of the diurnal cycle, the composites are plotted out to a radius of  $r = 30$  km, far enough away from the center that only the effects of the diurnal cycle should be present. It should also be noted that there is some contamination from the sea breeze within these composites. Although all identified cold pools form ahead of the sea breeze, some are overtaken by the sea breeze during the two subsequent hours for which they are included in the composite cold pool calculation.

Figures 2.16a and 2.16b show the evolution of the  $\theta_p$  and  $r_v$  fields, respectively. At  $t = -30$  minutes,  $\theta_p$  and  $r_v$  are both elevated near the center. At this time, the cold pool has not yet formed, and the elevated values of  $\theta_p$  and  $r_v$  indicate that convection preferentially develops near warm, moist perturbations within the domain. As the composite cold pool evolves, a  $\theta_p$  depression appears, peaking in strength around  $t = 0$  minutes, the time at which the cold pools in the composite are identified. The magnitude of the depression at this time is approximately 2.5 K. The original elevated values of  $\theta_p$  do not disappear entirely; they appear to be advected outward, forming a weak ring-like structure (i.e., a local maximum at some given radial coordinate) of enhanced  $\theta_p$  values. The  $\theta_p$  depression expands in radius as the composite cold pool grows in size, and as time progresses, the strength of the depression decreases. Meanwhile, the values of  $\theta_p$  away from the cold pool center decrease in association with the evening phase of the diurnal cycle. By  $t = 120$  minutes, the composite cold pool has dissipated, and the values of  $\theta_p$  near the cold pool center are similar to those away from the cold pool center.

In the  $r_v$  field, interesting trends emerge. Initially, the moist perturbation near the center expands; this expansion is likely due to the evaporation of precipitation (Figure 2.16d). Subsequently, a moisture ring appears: there are low values of  $r_v$  closest to the cold pool center, surrounded by significantly enhanced values of  $r_v$  around the periphery of the cold pool. The low

values of  $r_v$  near the center are likely the result of strong, penetrating downdrafts transporting dry air from aloft.

A ring-like structure also appears in the  $\theta_e$  field, shown in Figure 2.16c. In agreement with the  $\theta_\rho$  and  $r_v$  composites, there are enhanced values of  $\theta_e$  at the center at  $t = -30$  minutes. Then, a  $\theta_e$  depression emerges in the center, and a ring of enhanced  $\theta_e$  propagates outward. The maximum magnitude of the  $\theta_e$  depression is approximately 4 K.

The cold pool also affects the surface sensible and latent heat flux fields, shown in Figures 2.16e and 2.16f, respectively. Initially, both the sensible and latent heat fluxes are suppressed near the center. This is due to shading from the cold pool's parent cloud; the lack of downwelling shortwave radiation translates into a lack of energy available to power the surface fluxes. Simultaneously, a ring-like structure appears in the latent heat flux composite, as well as, to a lesser extent, in the sensible heat flux composite. This is the wind-induced enhancement of surface heat fluxes associated with the radial winds (Figure 2.17a). Away from the cold pool, both the sensible and latent heat fluxes decrease with time as the evening phase of the diurnal cycle approaches.

Figure 2.17a shows the evolution of the radial wind field. At  $t = -30$  minutes, before the formation of the cold pool, there is radial inflow associated with the cold pool's parent cloud. By  $t = 0$  minutes this has transitioned to radial outflow associated with the cold pool. The location of the peak radial wind moves outward over time as the cold pool expands. The expansion of the cold pool can also be seen in the horizontal  $\theta_\rho$  advection field in Figure 2.17b. The strength of the negative  $\theta_\rho$  advection decreases with time, as does the strength of the radial outflow. These trends may be due to cold pool weakening associated with surface fluxes (e.g., Grant and van den Heever 2016). Figure 2.17c shows the evolution of the pressure perturbation. At  $t = -30$

minutes, before the cold pool forms, there is a negative pressure perturbation. This is a hydrostatic low caused by the buoyant air aloft associated with the cold pool's parent cloud. Once the cold pool forms, the low-pressure perturbation is replaced by a high-pressure perturbation caused by a combination of hydrostatic and nonhydrostatic effects. There is nonhydrostatic high pressure near the center of the cold pool associated with the collision of downdraft air with the surface. There is also hydrostatic high pressure associated with the cool, dense cold pool air. The high-pressure perturbation persists, slowly decaying over the remainder of the cold pool lifecycle. Figures 2.17d-f show the evolution of the vertical motion. Before the formation of the cold pool, there are near-surface updrafts, consistent with inflow associated with the cold pool's parent cloud. Updrafts soon give way to downdrafts near cold pool center surrounded by updrafts away from the center of the cold pool. These results are consistent with the results presented in Section 2.4.

### 2.6.2 Moist Patch

One feature that appears in several of the fields is what we will term a *moist patch*. The moist patch is a region in which the ground has been soaked by precipitation and which has greater thermal inertia as a result. As time progresses, the ground remains cool as precipitation evaporates, absorbing the latent heat of vaporization. The moist patch is visible in Figure 2.16e as a region of negative sensible heat fluxes. It is also visible in Figure 2.16f as a region of enhanced latent heat fluxes. The negative sensible heat fluxes cool the air, leading to a pocket within the cold pool of especially low  $\theta_p$ , which is visible in Figure 2.16a within the innermost 5 km. The enhanced latent heat fluxes moisten the air enough to create a region of enhanced  $r_v$ , and indeed, there is a progression over time in Figure 2.16b from a ring-like structure, in which  $r_v$  is maximized at some outer radius, to a structure in which  $r_v$  is maximized near the center of

the cold pool. Since these processes are approximately moist-adiabatic, the moist patches are difficult to discern in the  $\theta_e$  field.

The role of the moist patch is to delay the recovery of the cold pool to background environmental temperatures, particularly within the center of the cold pool. The result is that new convection is especially suppressed in this region. In the early stages of cold pool growth, the moist patch has a secondary role. The soaking of the ground flips the sign of the surface sensible heat fluxes, and so when the gust front passes over the moist patch, the wind induces especially strong *negative* surface sensible heat fluxes rather than especially strong *positive* surface sensible heat fluxes. As a result, the sensible heat fluxes serve to strengthen the cold pool rather than weaken it within this region. This effect can be seen in the asymmetry of the  $v_r$  field in Figure 2.7c, which corresponds to the surface sensible heat flux field in Figure 2.8c.

In simulations, the moist patch may only exist when it is possible for the ground to be soaked and for the surface fluxes to respond. This is the value of using a model like RAMS that includes a coupled, interactive land surface scheme.

## 2.7 Defining Cold Pool Depth

One goal that the cold pool identification and tracking methods presented in Section 2.5 do not accomplish is defining convective cold pool depth. Accomplishing this goal is beyond the scope of the present work. However, the convective cold pool composites do provide some clues as to the particular features that define the tops of convective cold pools.

One potential metric for defining the tops of convective cold pools is the radial velocity,  $v_r$ . The radial velocity associated with the cold pool should be directed outward, and thus any radial inflow might be defined to be outside the cold pool. Figures 2.18 and 2.19 show composite cross-sections of  $\theta_p$  and radial velocity, respectively, at  $t = 0, 15, 30, 45,$  and 60 minutes. The

zero-contour in the radial velocity field is one potential cold pool upper boundary. This idea mirrors the method used by *Wilbanks et al.* [2015] to determine cold pool depth. However, some parts of the cold pool may have radial velocity directed inward, particularly within the density current “head” [cf. Figure 2 of *Goff*, 1976]. In this case, the entire depth of the cold pool may be better represented by the depth of negative tangential vorticity. Composite cross-sections of tangential vorticity are shown in Figure 2.20. This method results in significantly greater cold pool depth than does the method using radial velocity. It is difficult to discern from Figure 2.18 which method’s upper boundary is more appropriate.

## **2.8 Summary and Conclusions**

In this paper, we have reviewed the techniques that previous works have used to define convective cold pools, and we have then set out to develop a new approach to identifying convective cold pools in numerical simulations. First, cold pool structure is investigated in terms of a variety of different state variables based on simulated cold pools. This investigation highlights features, such as sharp gradients in density potential temperature, that define cold pool edges. Based on this analysis, we then develop a novel approach to identifying and tracking convective cold pools in numerical model simulations. This approach differs from previous approaches in that it is able both to differentiate between connected convective cold pools and to determine cold pool edges without the use of an arbitrary buoyancy or other threshold (with the exception of initial rainfall rates). The cold pool identification and tracking algorithm is applied to a numerical simulation of tropical convection, and a composite cold pool is generated and analyzed.

The results of both the initial and composite analyses generally agree with previous studies showing lowered temperatures, rings of enhanced water vapor, and enhanced radial

winds. One novel result, made possible by the use of an interactive land surface model, is the appearance of a moist patch in the later stages of the cold pool lifecycle. The moist patch is formed by the evaporation of rainwater off of a surface that has been soaked by precipitation during the initial stages of the cold pool lifecycle. The moist patch is characterized by the following characteristics:

- (i) negative sensible heat fluxes,
- (ii) enhanced latent heat fluxes,
- (iii) cool temperatures,
- (iv) enhanced water vapor, and
- (v) enhanced sinking motion.

The negative sensible heat fluxes prevent the recovery of temperature to that of the background environment within the moist patches, thus helping to prevent the formation of convection within the cold pool during this time period.

The cold pool identification algorithm is based on two variables: the surface rainfall rate and the density potential temperature. Both of these variables relate to physical processes in the cold pool. Rainfall is necessary in order to initiate a convective cold pool; without rainfall there is no evaporative cooling, and without significant surface rainfall, penetrating downdrafts are unlikely [*Barnes and Garstang*, 1982]. Cold pool edges are density currents [e.g., *Charba*, 1974], and thus the density potential temperature is directly related to cold pool propagation speed. The algorithm uses the rainfall field in order to identify regions in which a cold pool is likely to form, and the algorithm uses the density potential temperature field to identify cold pool edges. The edges are identified using the zero-contour of the second radial derivative of density

potential temperature, and thus the difficult task of determining a buoyancy threshold for defining cold pool edges is avoided.

The cold pool identification algorithm is not without limitations. The algorithm requires the specification of a somewhat arbitrary rainfall rate cutoff, and it does not attempt to quantify cold pool depth. Another limitation is that it assumes that systems are approximately stationary. It is difficult to anticipate how well the algorithm will perform in environments with greater shear or with more widespread precipitation. Furthermore, as with any numerical modeling endeavor, the validity of any results obtained using the cold pool identification algorithm is limited by the validity of the model being used to simulate the cold pools in question.

Nevertheless the algorithm does a remarkable job identifying cold pool edges, and it can be used to generate useful statistics about cold pool evolution. Importantly, this algorithm also provides a framework in which average cold pool properties can be compared from one simulation to the next. For example, efforts are currently underway to compare the cold pools examined here with ensembles of simulated cold pools in which the initial soil moisture is reduced.

## 2.9 Table and Figures

Table 2.1. RAMS model setup, adapted from Grant and van den Heever (2014).

<b>Model Aspect</b>	<b>Setting</b>
<b>Grid</b>	Arakawa C grid $\Delta x = \Delta y = 1 \text{ km}$ ; 550 km $\times$ 200 km domain size $\Delta z$ variable minimum $\Delta z = 100 \text{ m}$ , maximum $\Delta z = 1 \text{ km}$ vertical stretch ratio = 1.05 57 vertical levels; model top $\sim 26 \text{ km}$
<b>Time integration</b>	3 s time step; 16 h simulation duration
<b>Initialization</b>	Horizontally homogeneous thermodynamic and wind profile, averaged from ECMWF YOTC analysis data Initial start time 600 UTC 1 July Random thermal perturbations through lowest 2 km agl, with a maximum magnitude of 1 K at the lowest model level above ground
<b>Surface scheme</b>	LEAF-3 [ <i>Walko et al.</i> , 2000] 11 soil levels from 0.01 m to 0.5 m below ground Western third of domain: ocean (SST 300 K) Eastern two thirds of domain: evergreen broadleaf tree surface type, sandy clay loam soil type
<b>Boundary conditions</b>	Radiative lateral boundary [ <i>Klemp and Wilhelmson</i> , 1978] in zonal direction; periodic in meridional direction Rayleigh friction damping over top six vertical levels ( $\sim 21\text{--}26 \text{ km}$ agl)
<b>Microphysics scheme</b>	Two-moment bulk microphysics [ <i>Meyers et al.</i> , 1997] 8 hydrometeor classes [ <i>Saleeby and Cotton</i> , 2004]
<b>Radiation scheme</b>	<i>Harrington</i> [1997] two-stream, updated every 5 simulation minutes
<b>Aerosol treatment</b>	Aerosol species: sulfates [ <i>Saleeby and van den Heever</i> , 2013] No aerosol sources or sinks Aerosols radiatively active <i>DeMott et al.</i> [2010] ice nucleation parameterization
<b>Turbulence scheme</b>	<i>Smagorinsky</i> [1963] deformation K with stability modification by <i>Hill</i> [1974]; stability modifications by [ <i>Lilly</i> , 1962] used gradually above the boundary layer
<b>Coriolis</b>	No

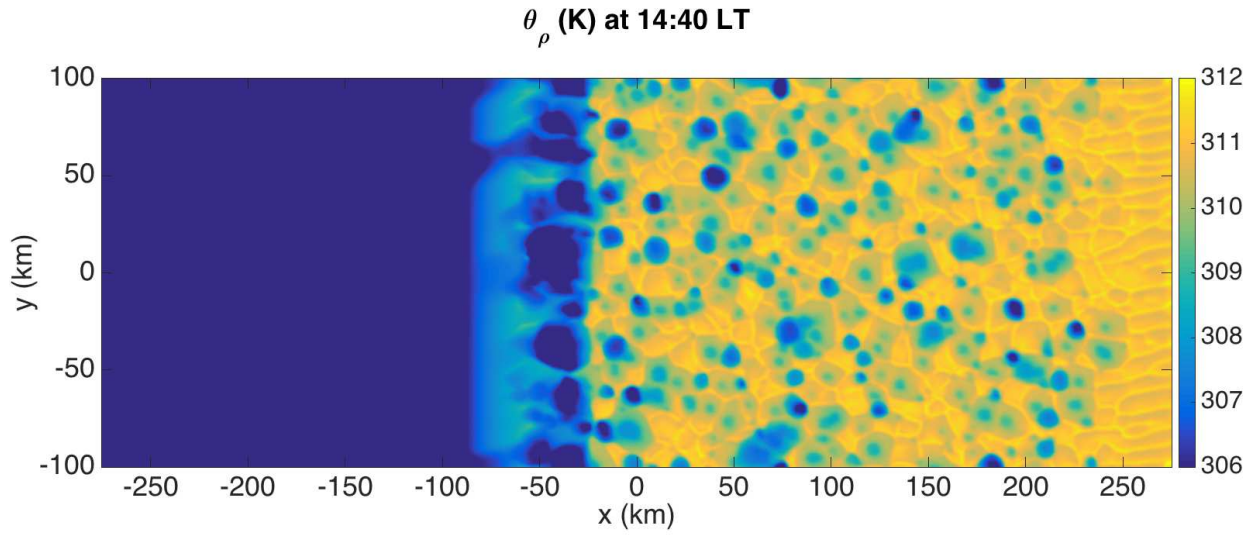


Figure 2.1. Snapshot of the  $\theta_\rho$  field at the lowest model level,  $z \sim 50$  m. The ocean-land boundary is at  $x \sim -92$  km, and the sea-breeze location is identified to be at  $x \sim -22$  km.

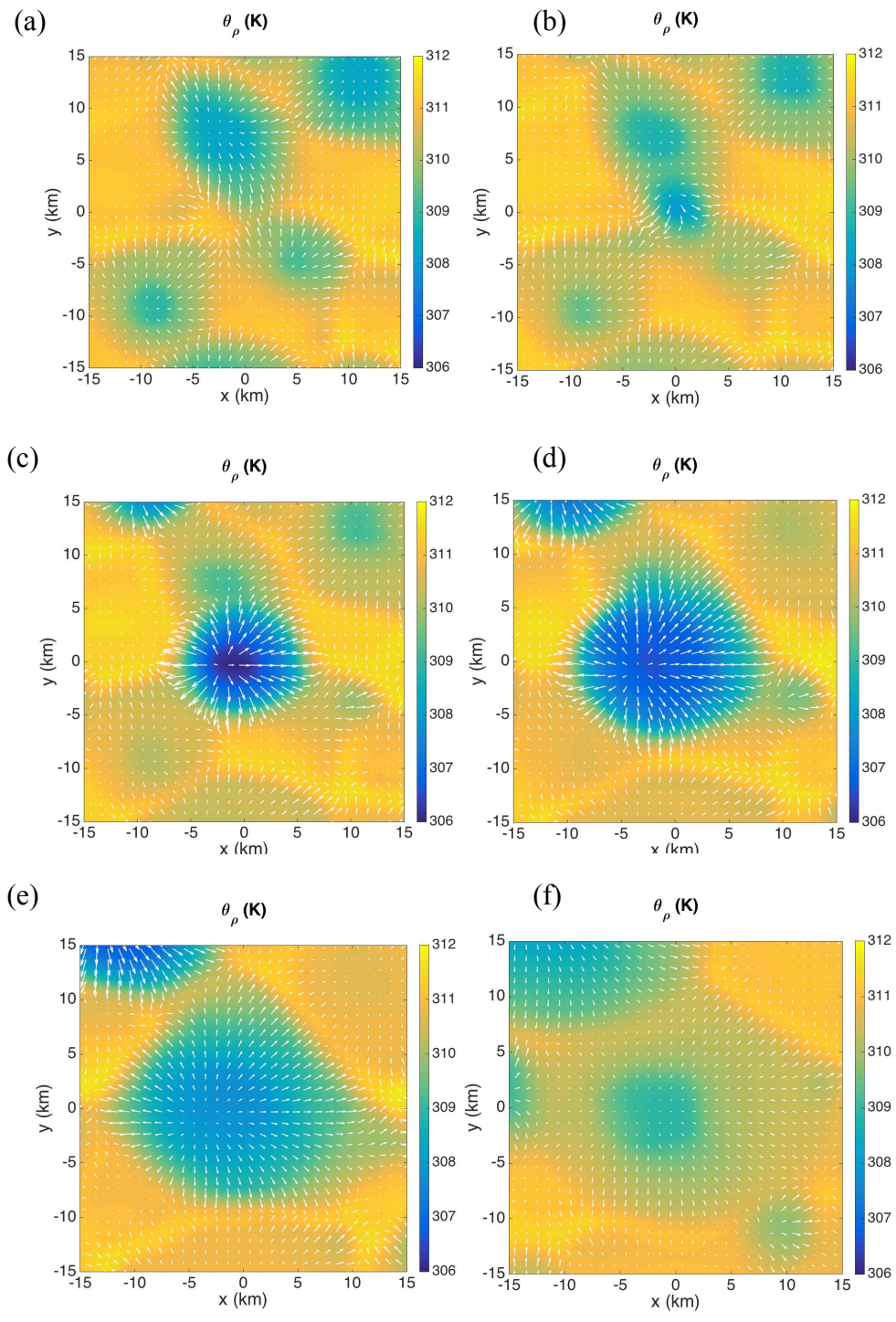


Figure 2.2. Evolution of the  $\theta_\rho$  field (colors) and horizontal winds (white arrows) at  $z \sim 50$  m for the sample cold pool: (a)  $t = -30$  minutes; (b)  $t = -15$  minutes; (c)  $t = 0$  minutes; (d)  $t = 15$  minutes; (e)  $t = 30$  minutes; (f)  $t = 75$  minutes. Horizontal coordinates are computed relative to the approximate center of the cold pool and thus differ from those in Figure 2.1.

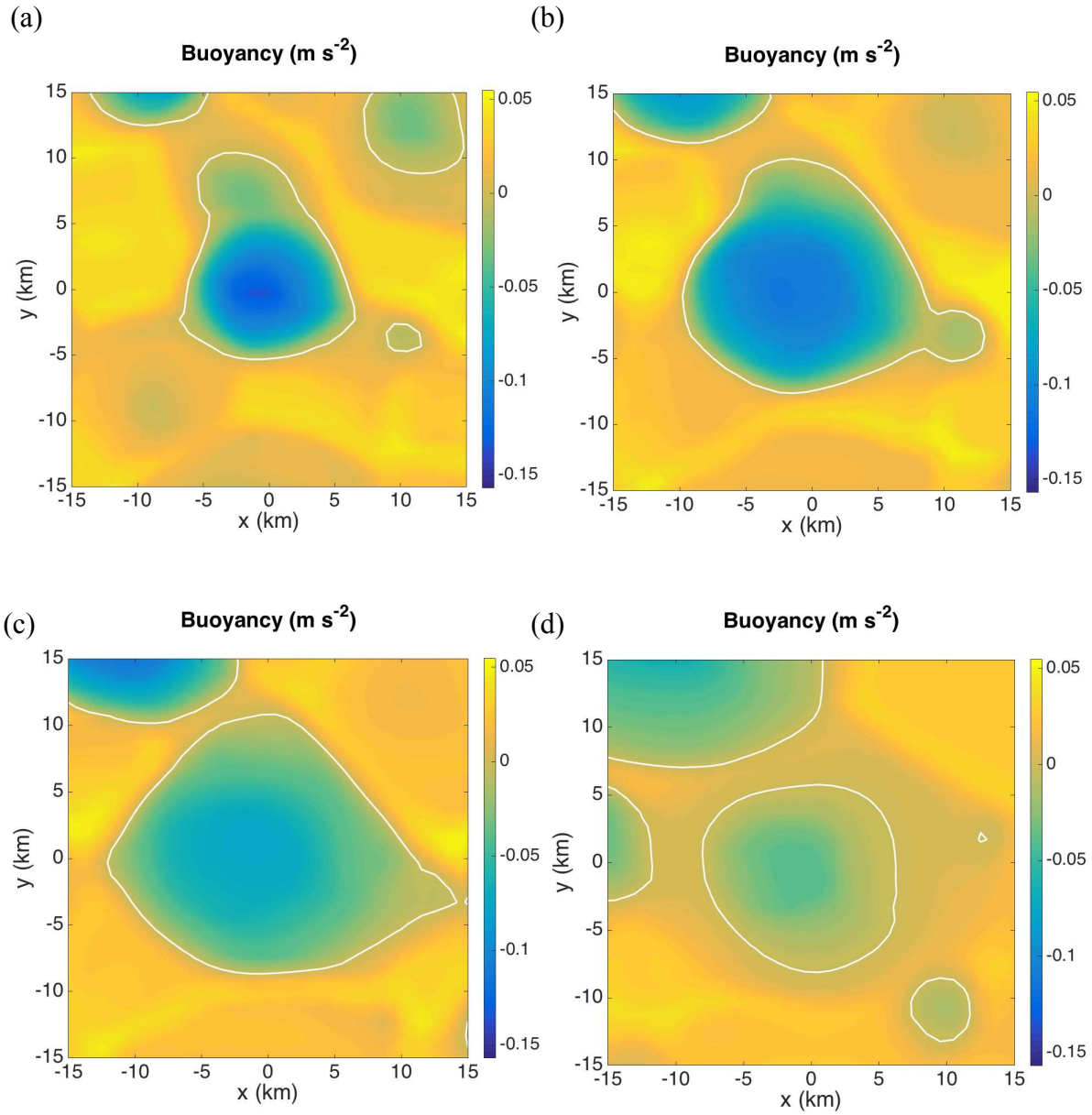


Figure 2.3. Buoyancy  $B$  at (a)  $t = 0$  minutes, (b)  $t = 15$  minutes, (c)  $t = 30$  minutes, and (d)  $t = 75$  minutes. Note that the area enclosed by the  $B = 0$  (plotted in white) contour decreases from (c) to (d).

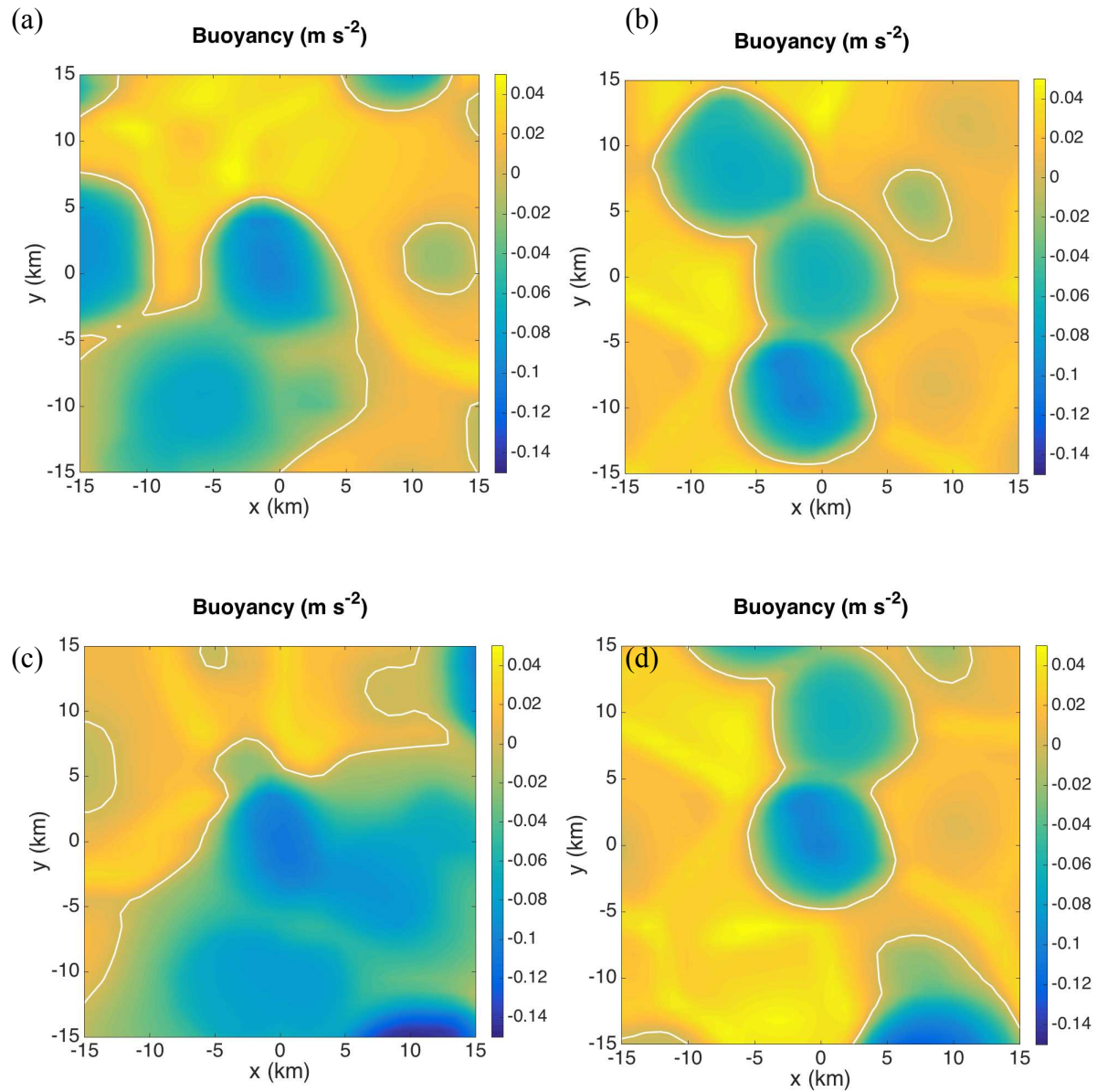


Figure 2.4. Buoyancy field for an assortment of colliding cold pools. The  $B = 0$  contour is plotted in white. Panels (b) and (d) show the same scene, each focusing on one of two colliding cold pools.

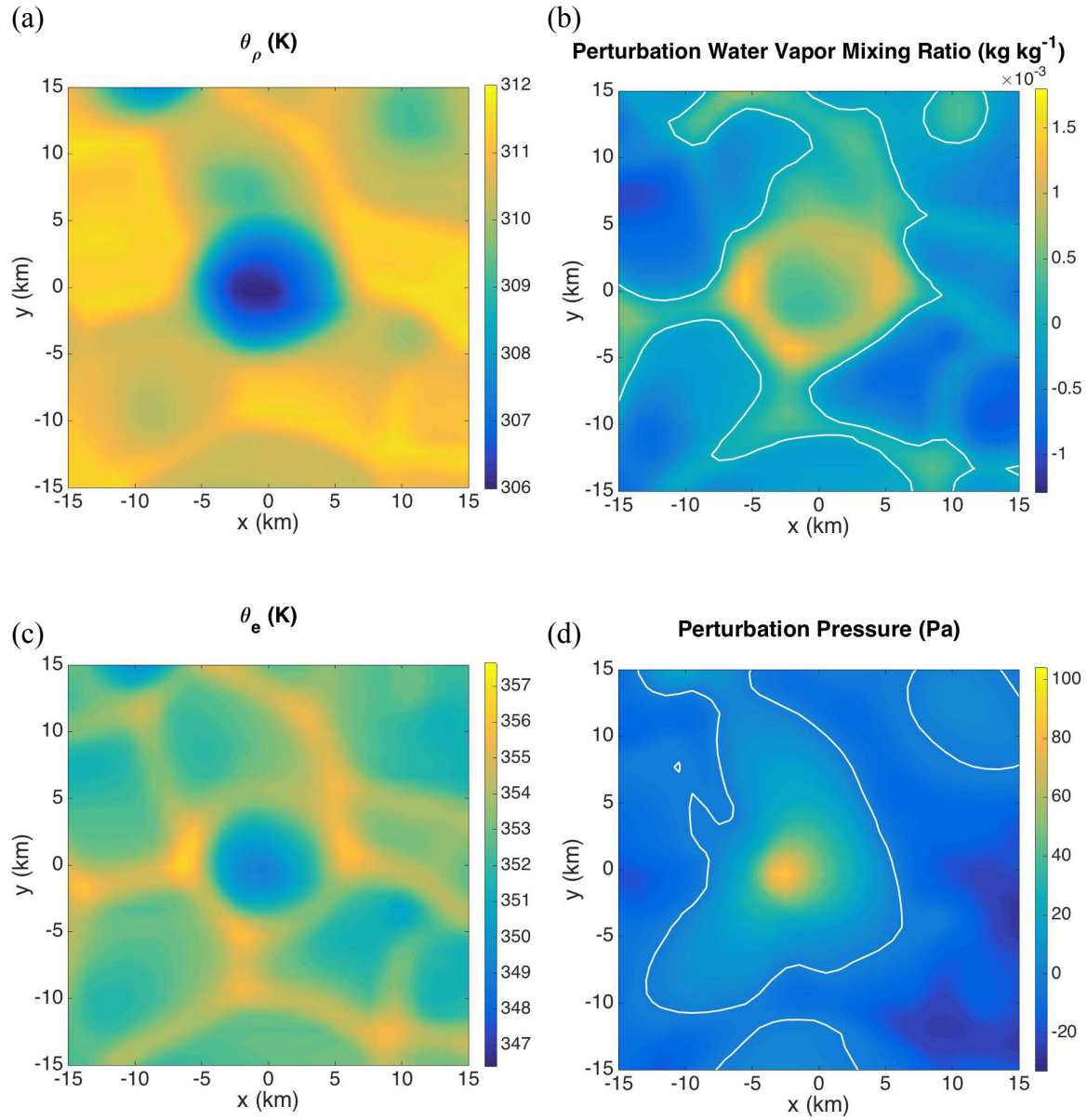


Figure 2.5. Various fields at  $t = 0$  minutes: (a) density potential temperature  $\theta_\rho$ , (b) perturbation water vapor mixing ratio  $r'_v$ , (c) equivalent potential temperature  $\theta_e$ , and (d) perturbation pressure  $p'$ . Zero-contours are plotted in white.

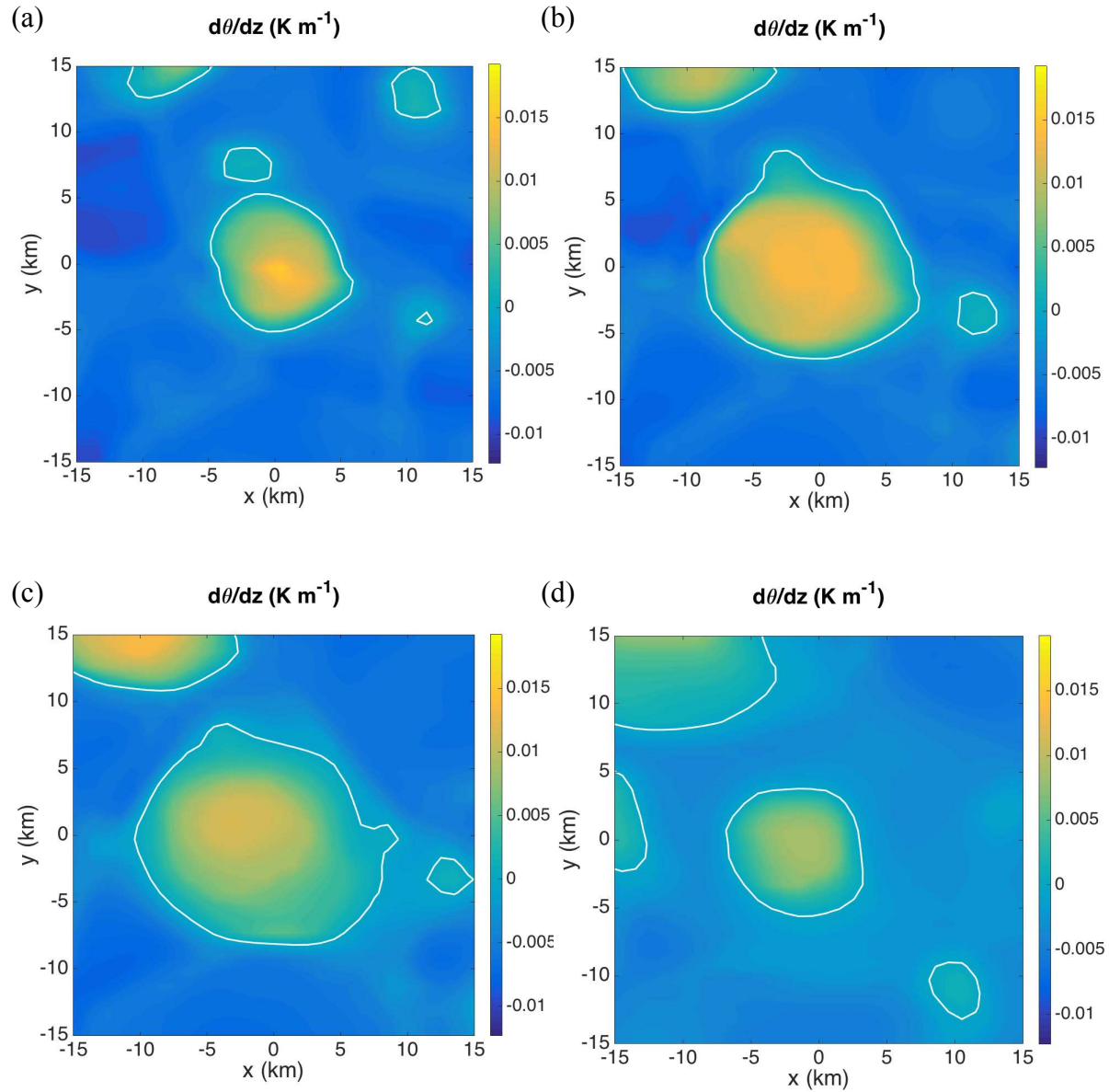


Figure 2.6. Static stability  $\frac{\partial\theta}{\partial z}$  at (a)  $t = 0$  minutes, (b)  $t = 15$  minutes, (c)  $t = 30$  minutes, and (d)  $t = 75$  minutes. Note that the area enclosed by the central  $\frac{\partial\theta}{\partial z} = 0$  contour (white) decreases from (c) to (d).

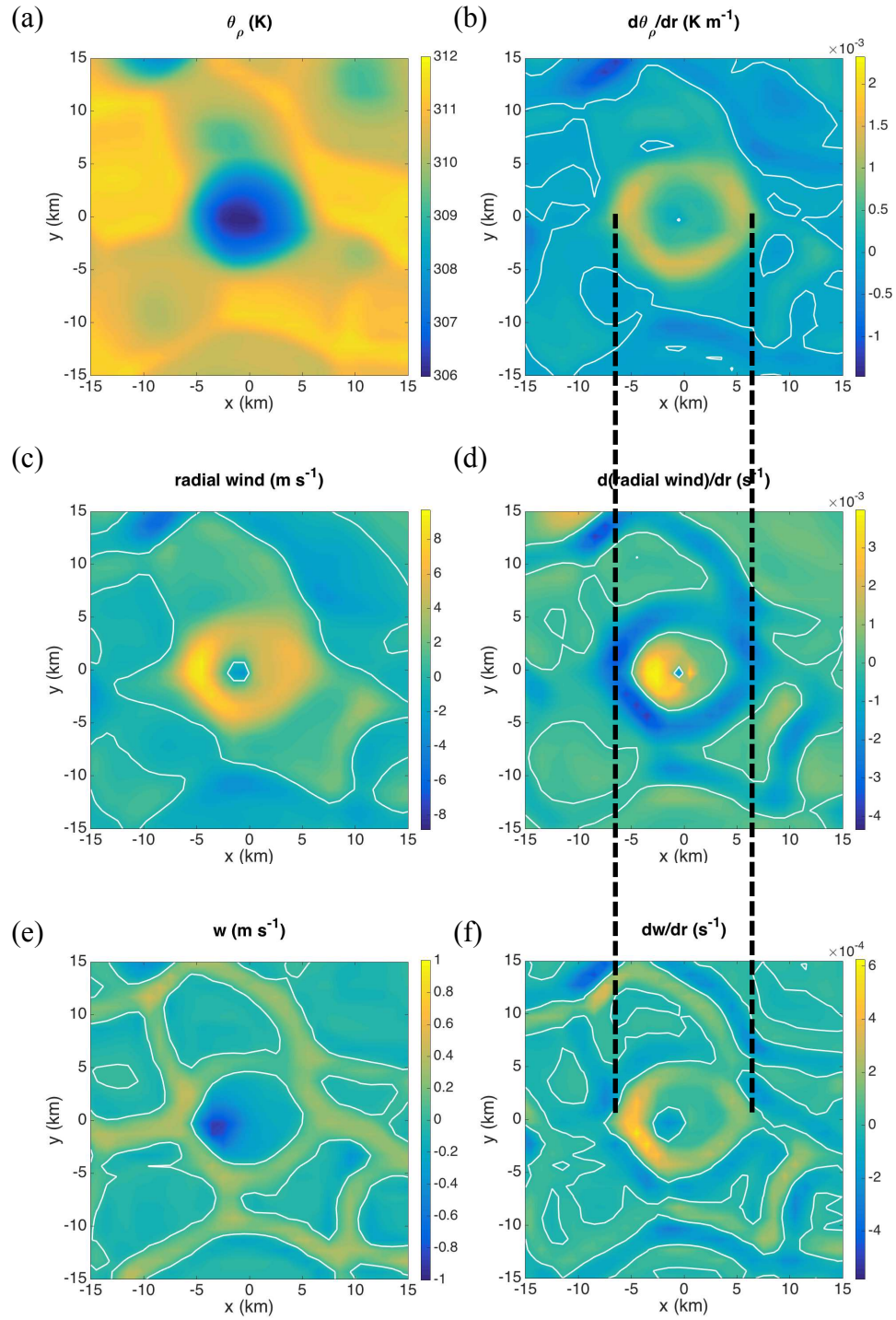


Figure 2.7. Three variables and their radial derivatives at  $t = 0$  minutes: (a) density potential temperature  $\theta_\rho$ , (b)  $\frac{\partial \theta_\rho}{\partial r}$ , (c) radial velocity  $v_r$ , (d)  $\frac{\partial v_r}{\partial r}$ , (e) vertical velocity  $w$ , and (f)  $\frac{\partial w}{\partial r}$ . The vertical dashed black lines are shown to facilitate comparison between panels (b), (d), and (f). Note that the radial gradients in  $v_r$  are located radially outward from the radial gradients in  $\theta_\rho$  and  $w$ .

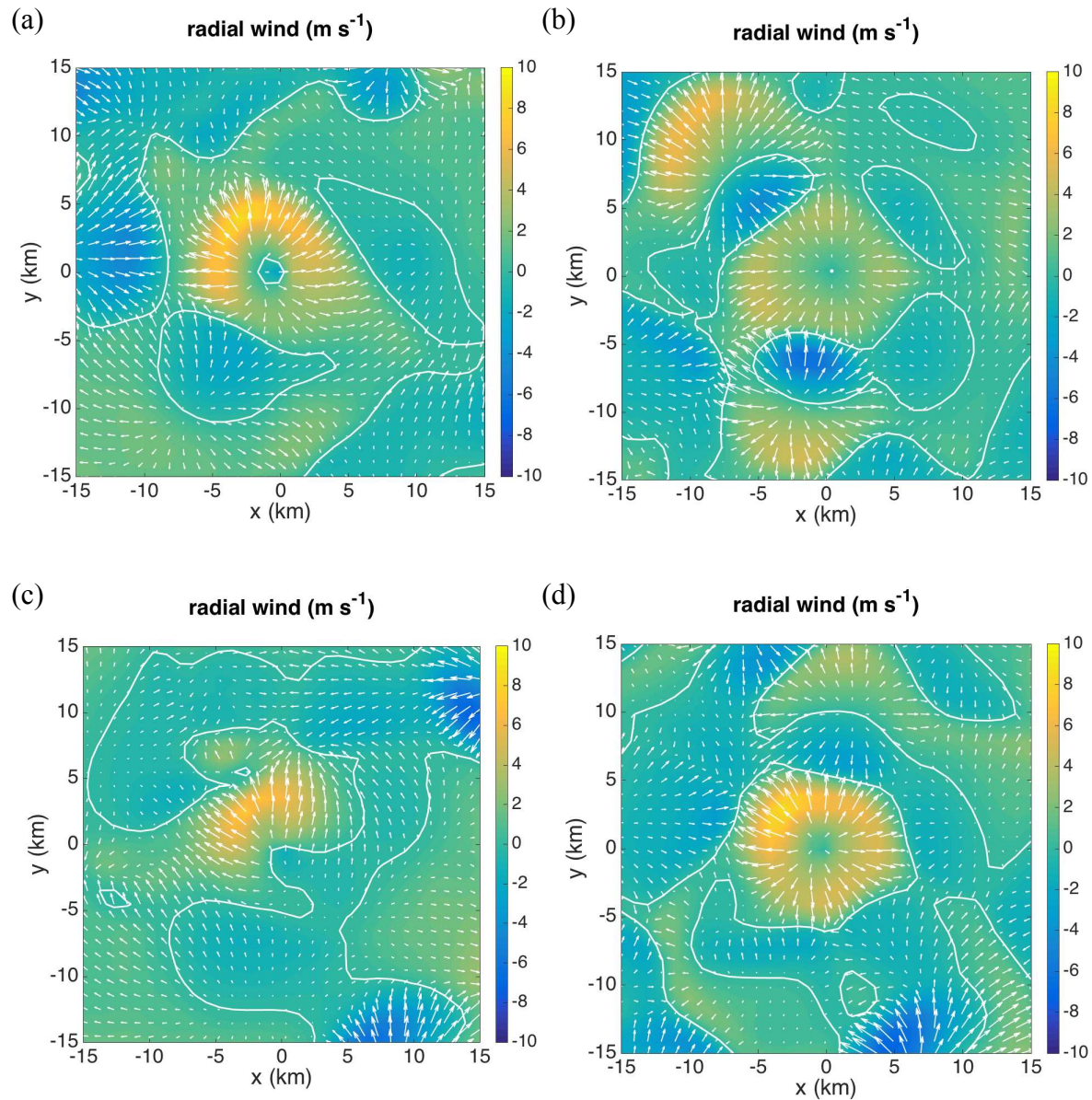


Figure 2.8. Radial velocity  $v_r$  (colors) and horizontal wind vectors (white) at  $z \sim 50$  m for the colliding cold pool scenes shown in Figure 2.4. In each panel, the radial velocity is computed relative to the approximate center of the centermost cold pool in the scene.

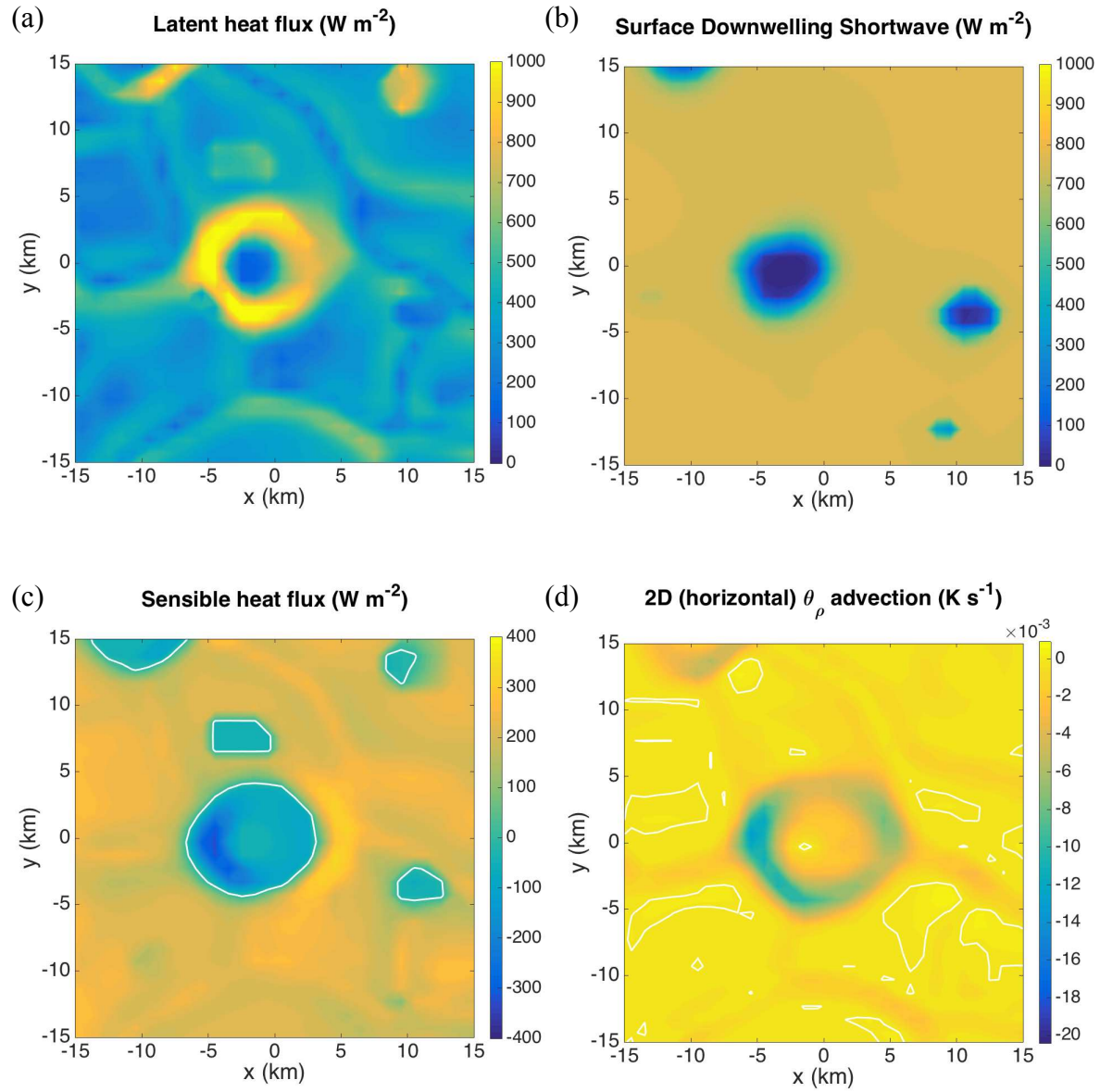


Figure 2.9. Various fields at  $t = 0$  minutes: (a) surface latent heat flux, (b) downwelling shortwave radiation at the surface (c) surface sensible heat flux, and (d) horizontal density potential temperature advection  $-\vec{v}_H \cdot \vec{\nabla}_H \theta_\rho$ .

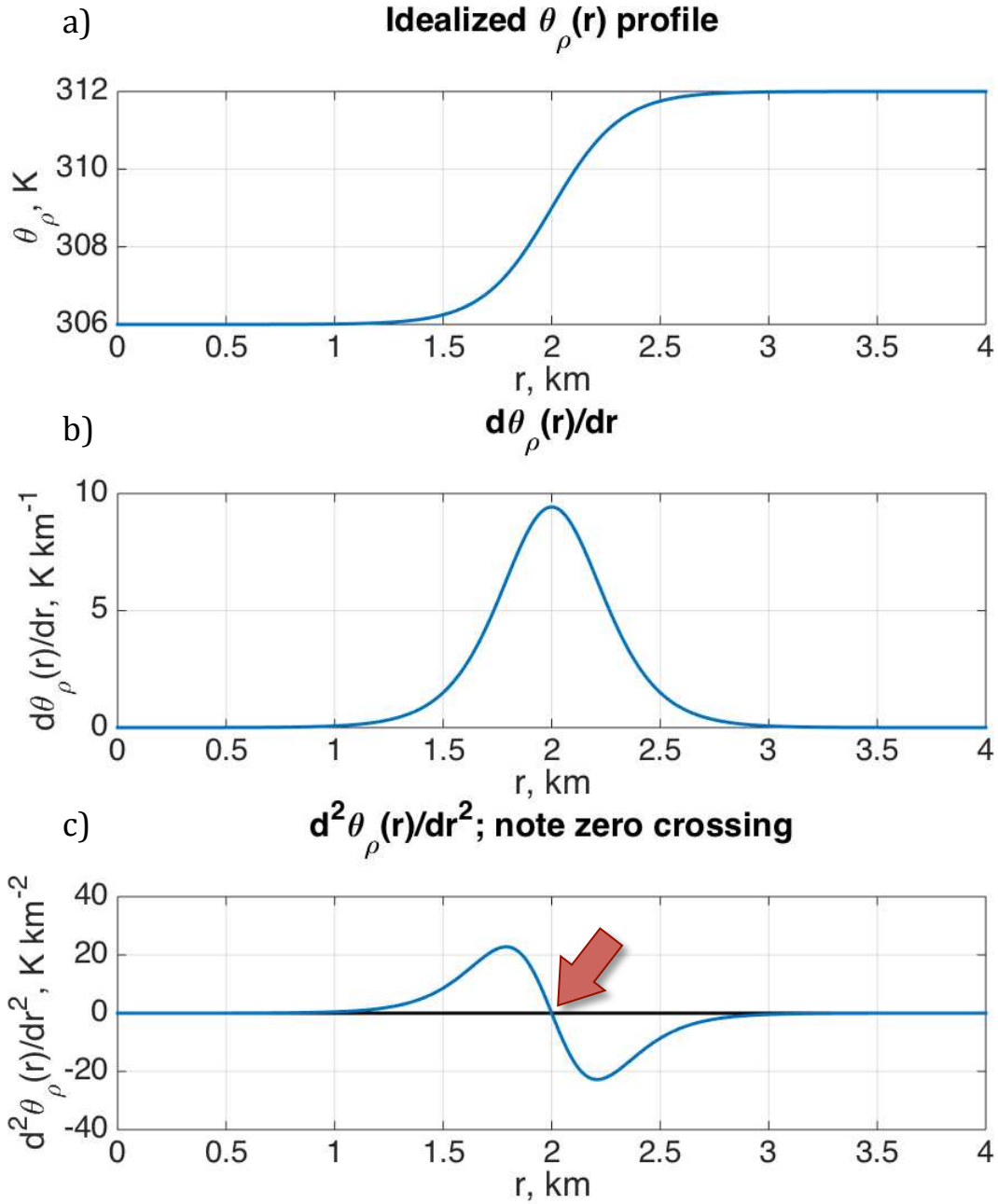


Figure 2.10. Idealized illustration of the reasoning behind using the second radial derivative: (a)  $\theta_\rho$ , (b)  $\frac{\partial\theta_\rho}{\partial r}$ , and (c)  $\frac{\partial^2\theta_\rho}{\partial r^2}$ .

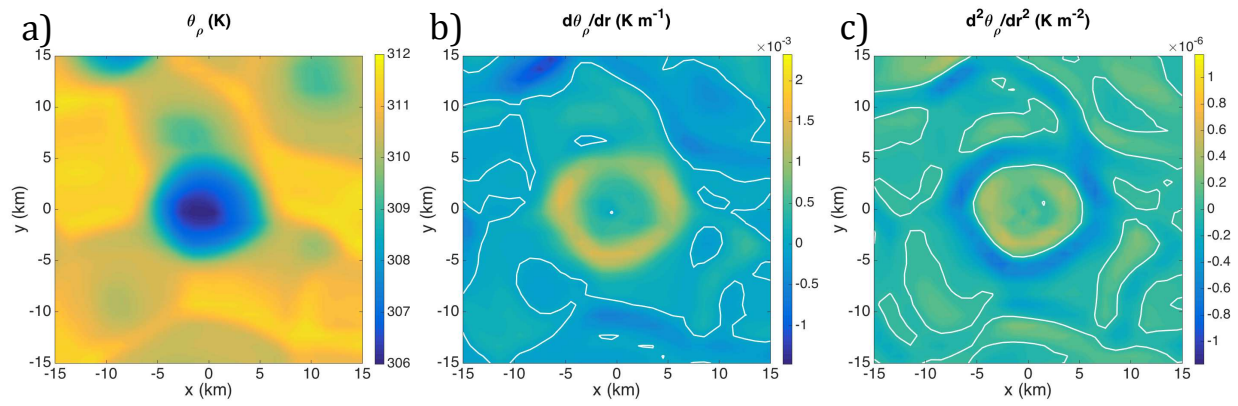


Figure 2.11. Illustration of the reasoning behind using the second radial derivative using the cold pool examined earlier: (a)  $\theta_\rho$ , (b)  $\frac{\partial\theta_\rho}{\partial r}$ , and (c)  $\frac{\partial^2\theta_\rho}{\partial r^2}$ .

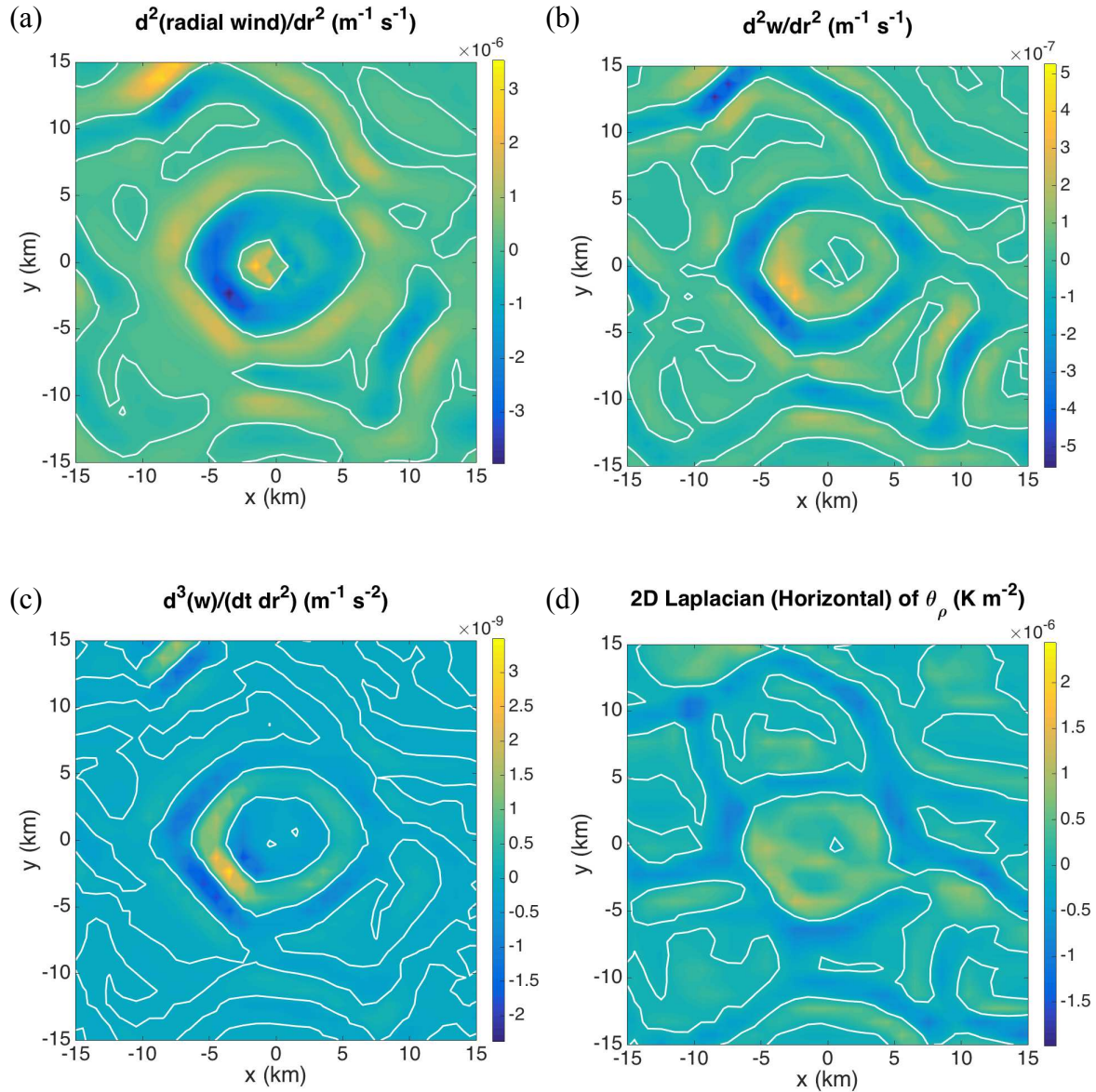


Figure 2.12. Alternative variables that were considered for identifying cold pool edges, all at  $t = 0$  minutes: (a)  $\frac{\partial^2 v_r}{\partial r^2}$ , (b)  $\frac{\partial^2 w}{\partial r^2}$ , (c)  $\frac{\partial^2}{\partial r^2} \left( \frac{\partial w}{\partial t} \right)$ , and (d)  $\nabla_H^2 \theta_\rho$ . Zero-contours are shown in white.

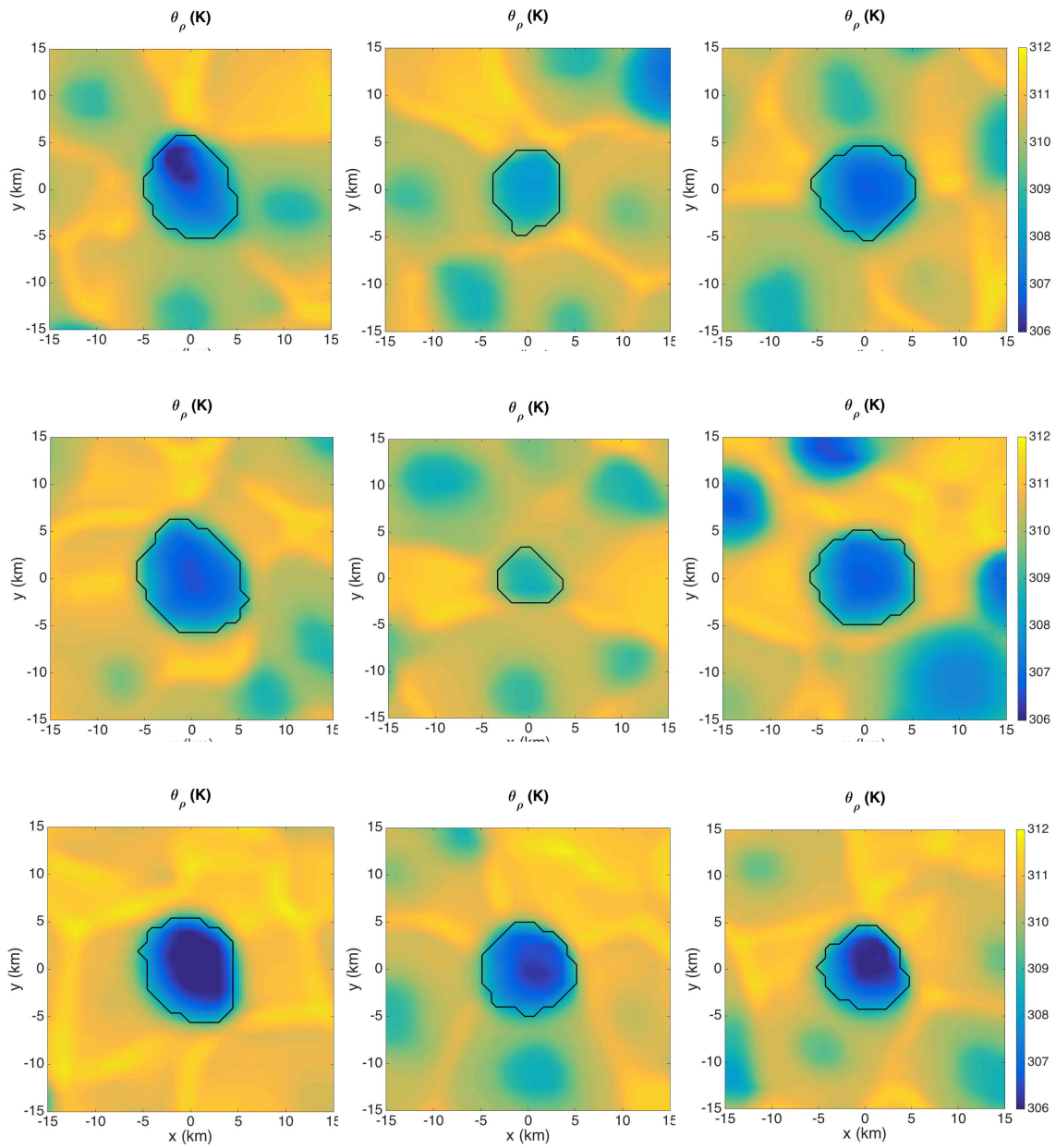


Figure 2.13. Algorithm performance for nine sample cold pools. Algorithm-derived boundaries are in black. All boundary locations have been rounded to the nearest pixel.

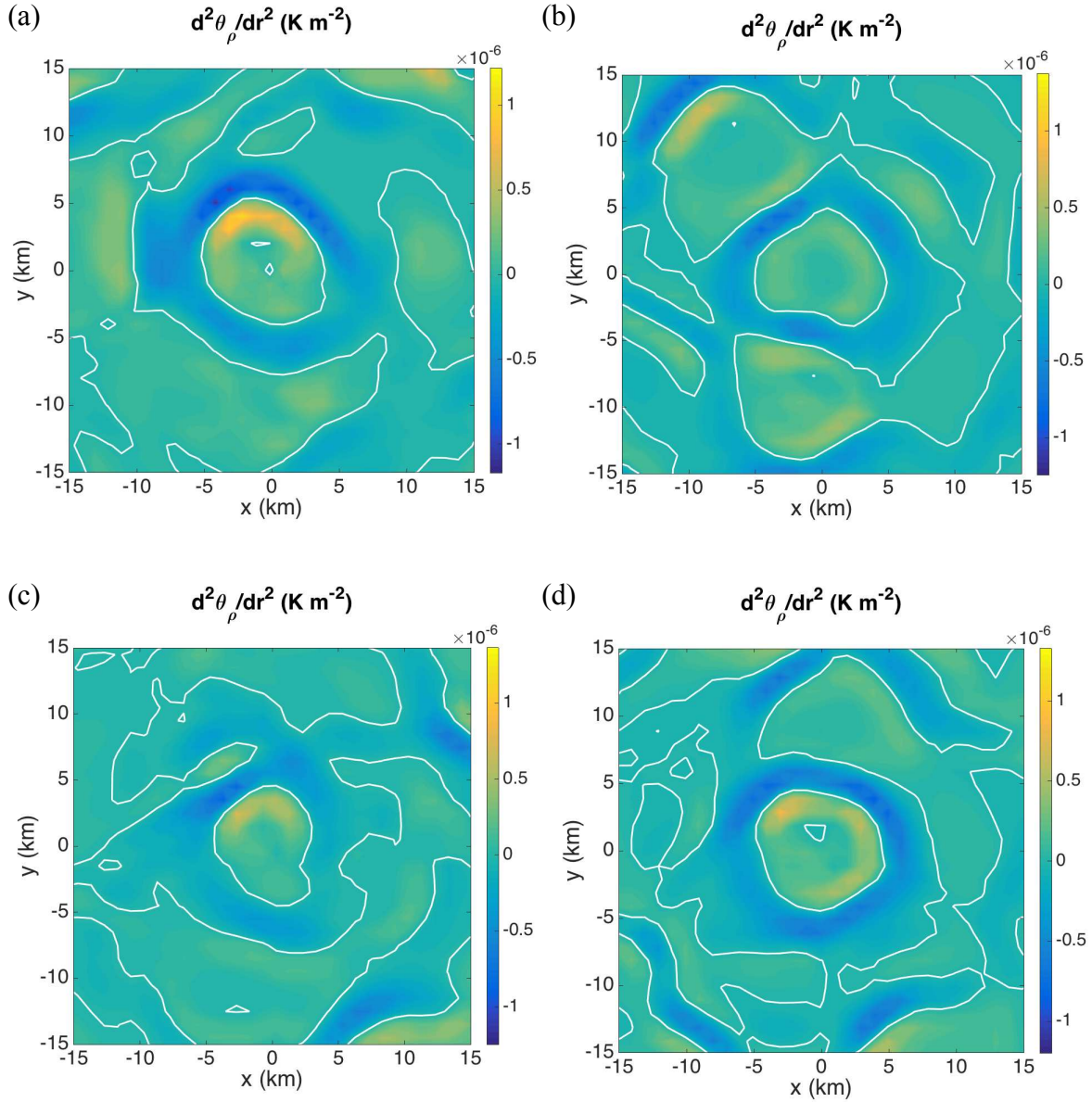


Figure 2.14. Algorithm performance for the connected cold pool scenes shown in Figure 2.4. Zero-contours of  $\frac{\partial^2\theta_\rho}{\partial r^2}$  are in white. The centermost contour is the boundary of the centermost cold pool.

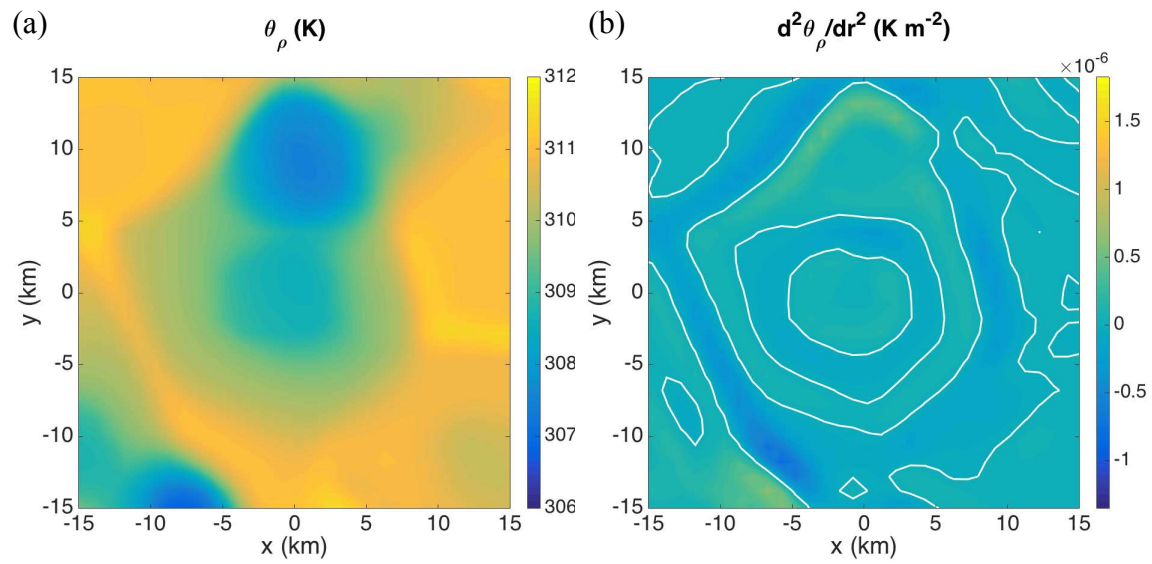


Figure 2.15. Case in which algorithm does not perform well: (a)  $\theta_\rho$  field; (b) corresponding  $\frac{\partial^2 \theta_\rho}{\partial r^2}$  field with the zero contour in white.

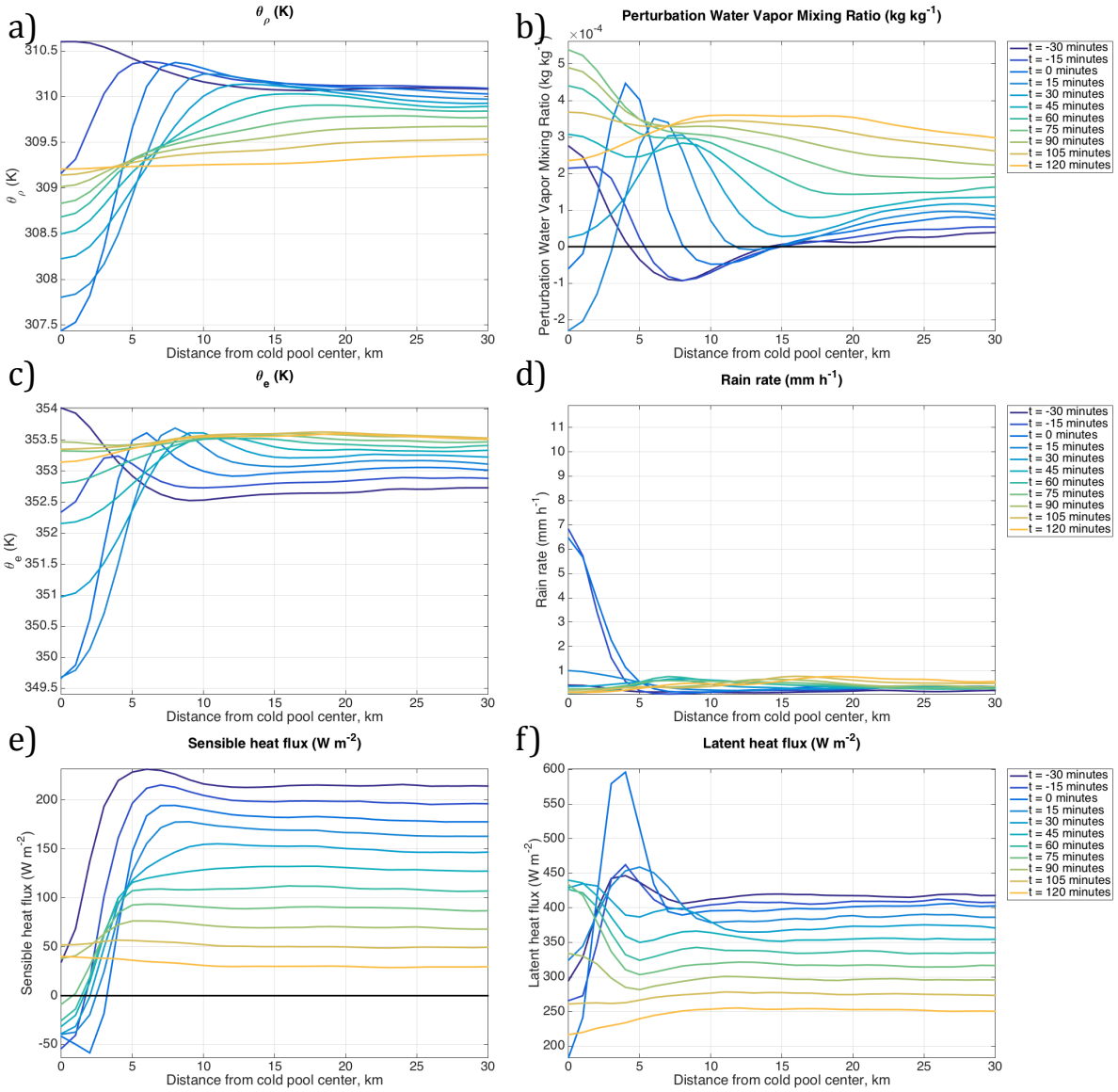


Figure 2.16. Composite time evolution of various thermodynamic and moisture variables: (a) density potential temperature  $\theta_\rho$  at  $z \sim 50$  m, (b) water vapor mixing ratio  $r_v$  at  $z \sim 50$  m, (c) equivalent potential temperature  $\theta_e$  at  $z \sim 50$  m, (d) surface rainfall rate, (e) surface sensible heat flux, and (f) surface latent heat flux.

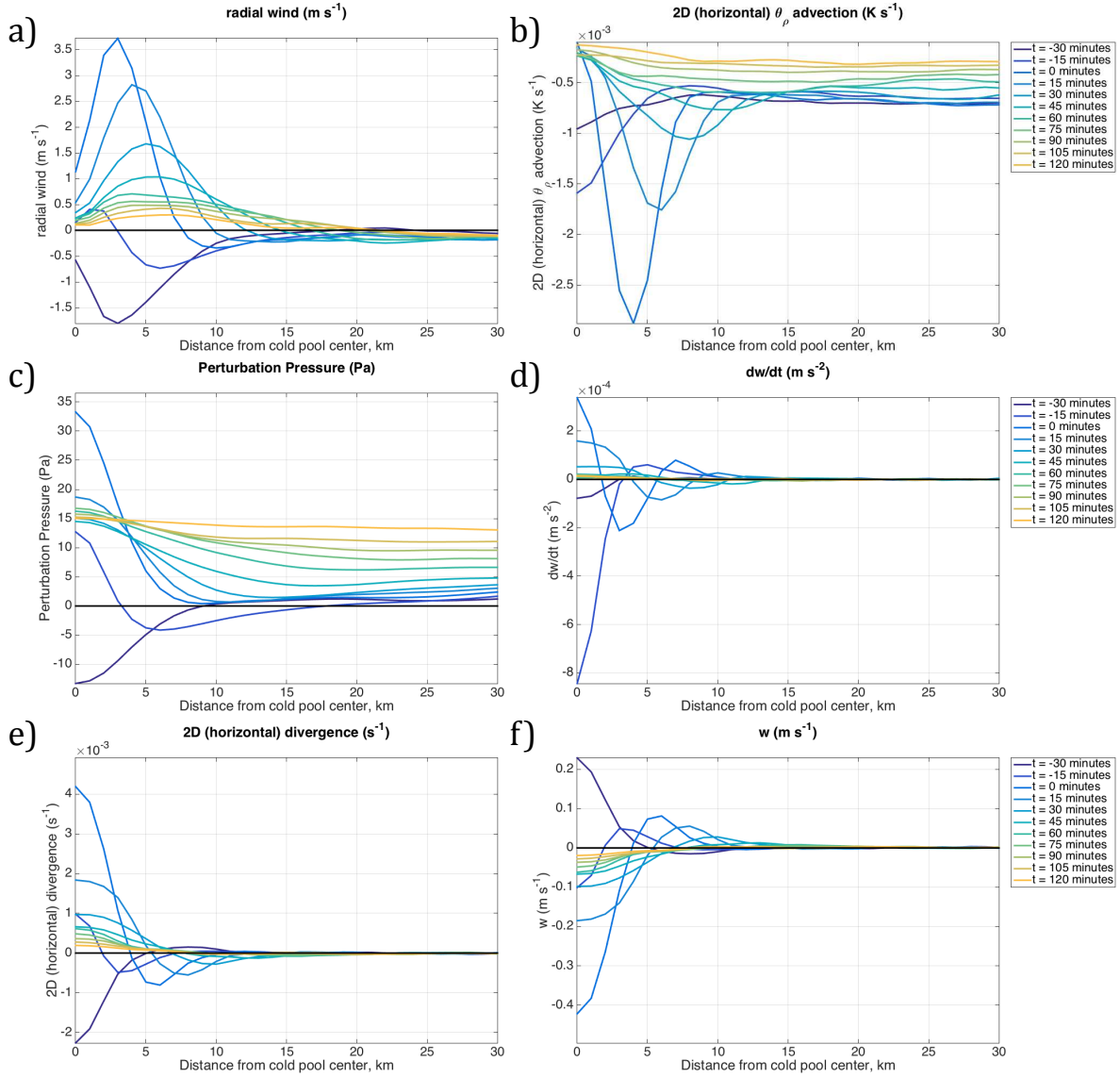


Figure 2.17. Composite time evolution of various dynamic variables: (a) radial wind  $v_r$  at  $z \sim 50$  m, (b) horizontal  $\theta_\rho$  advection at  $z \sim 50$  m, (c) perturbation pressure  $p'$  at  $z \sim 50$  m, (d) instantaneous vertical acceleration  $\frac{\partial w}{\partial t}$  at  $z = 100$  m, (e) horizontal wind divergence at  $z \sim 50$  m, and (f) vertical velocity  $w$  at  $z = 100$  m.

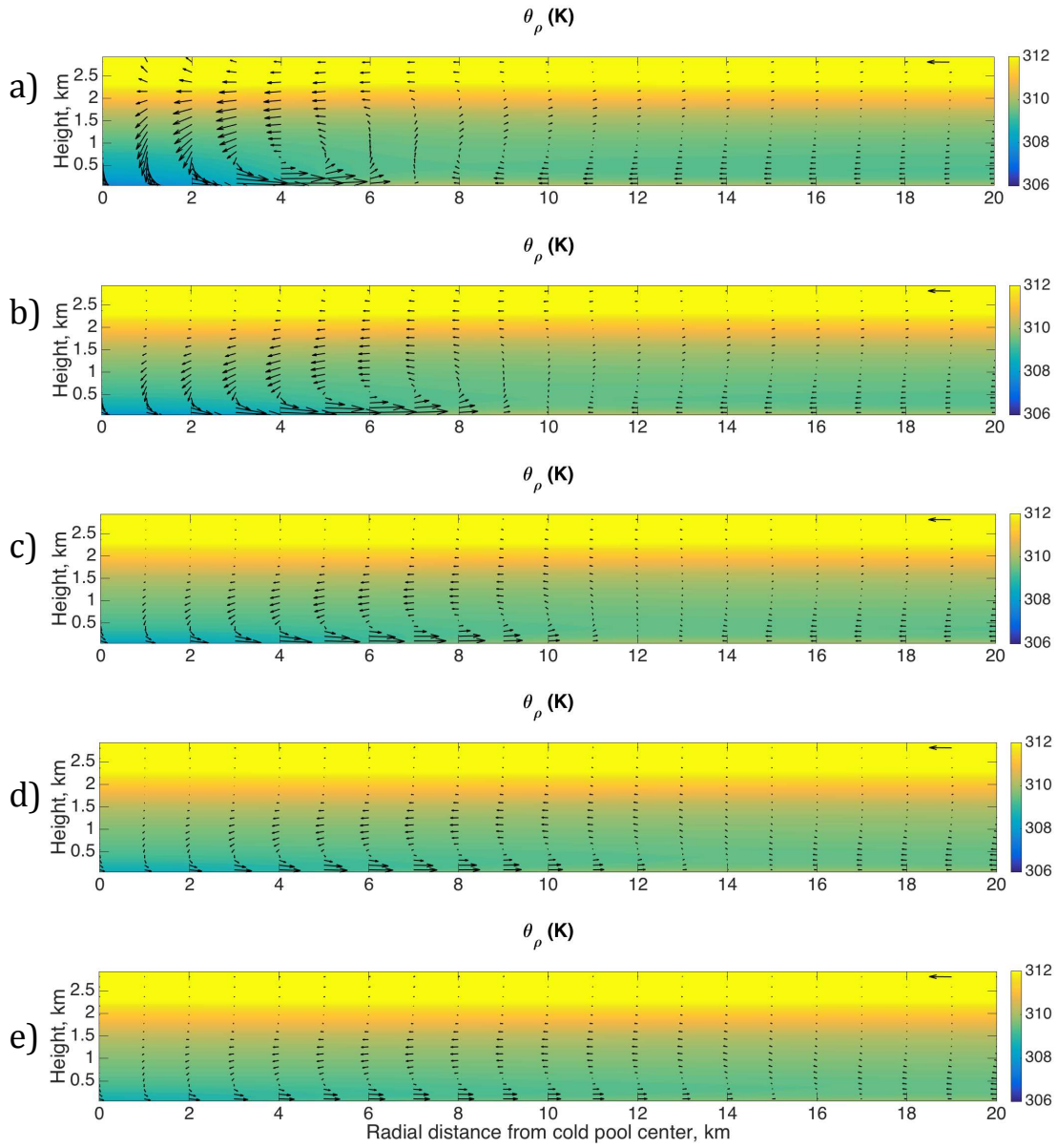


Figure 2.18. Composite cross-sections of  $\theta_\rho$  (colors) and the average transverse (radial and vertical) circulation (arrows) at (a)  $t = 0$  minutes, (b)  $t = 15$  minutes, (c)  $t = 30$  minutes, (d)  $t = 45$  minutes, and (e)  $t = 60$  minutes. The leftward-pointing arrow in the upper-right corner has a magnitude of  $1 \text{ m s}^{-1}$ .

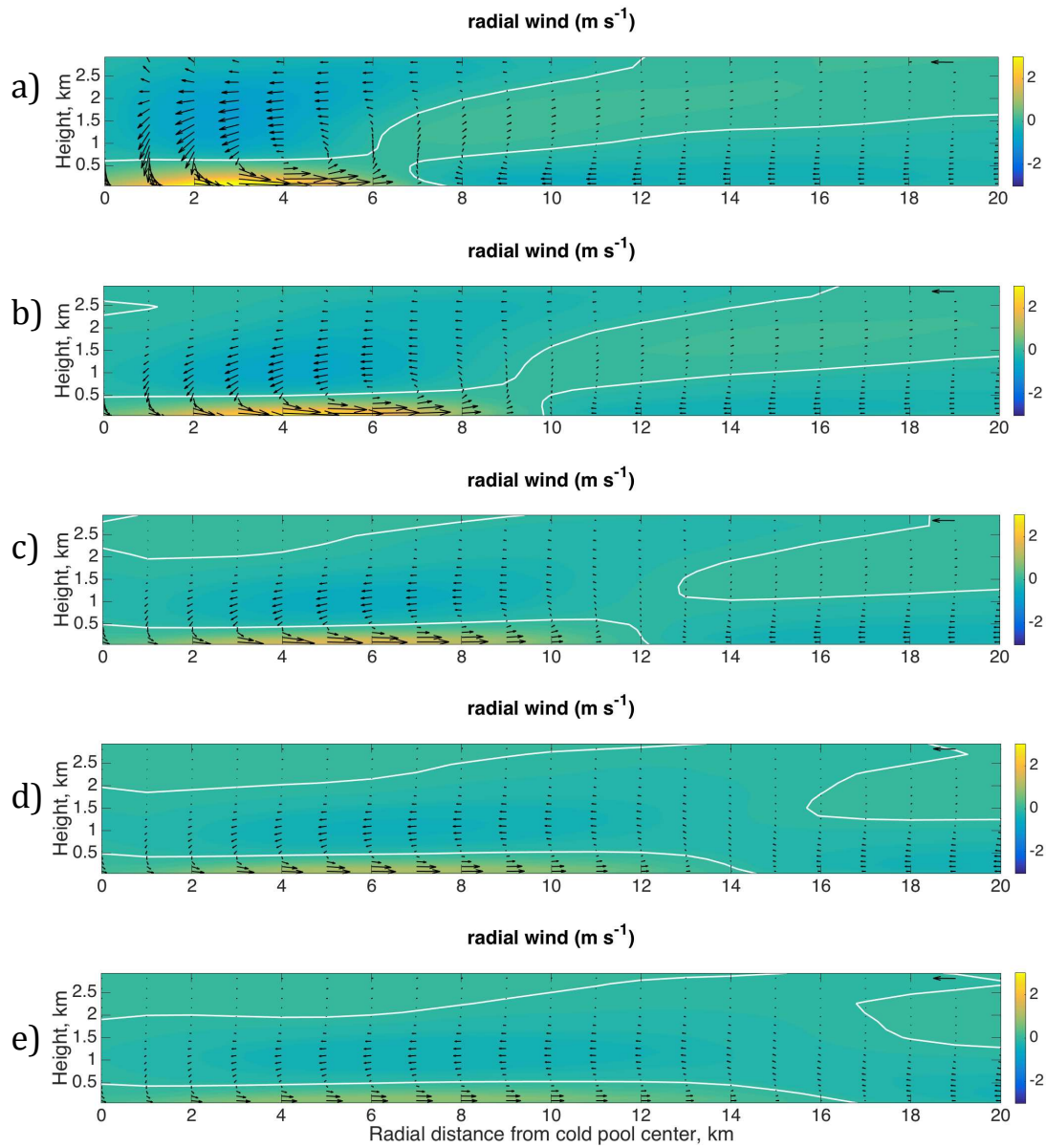


Figure 2.19. Composites of radial wind (colors) and transverse circulation (arrows) at (a)  $t = 0$  minutes, (b)  $t = 15$  minutes, (c)  $t = 30$  minutes, (d)  $t = 45$  minutes, and (e)  $t = 60$  minutes. The leftward-pointing arrow in the upper-right corner has a magnitude of  $1 \text{ m s}^{-1}$ . The zero-contour of radial wind is plotted in white.

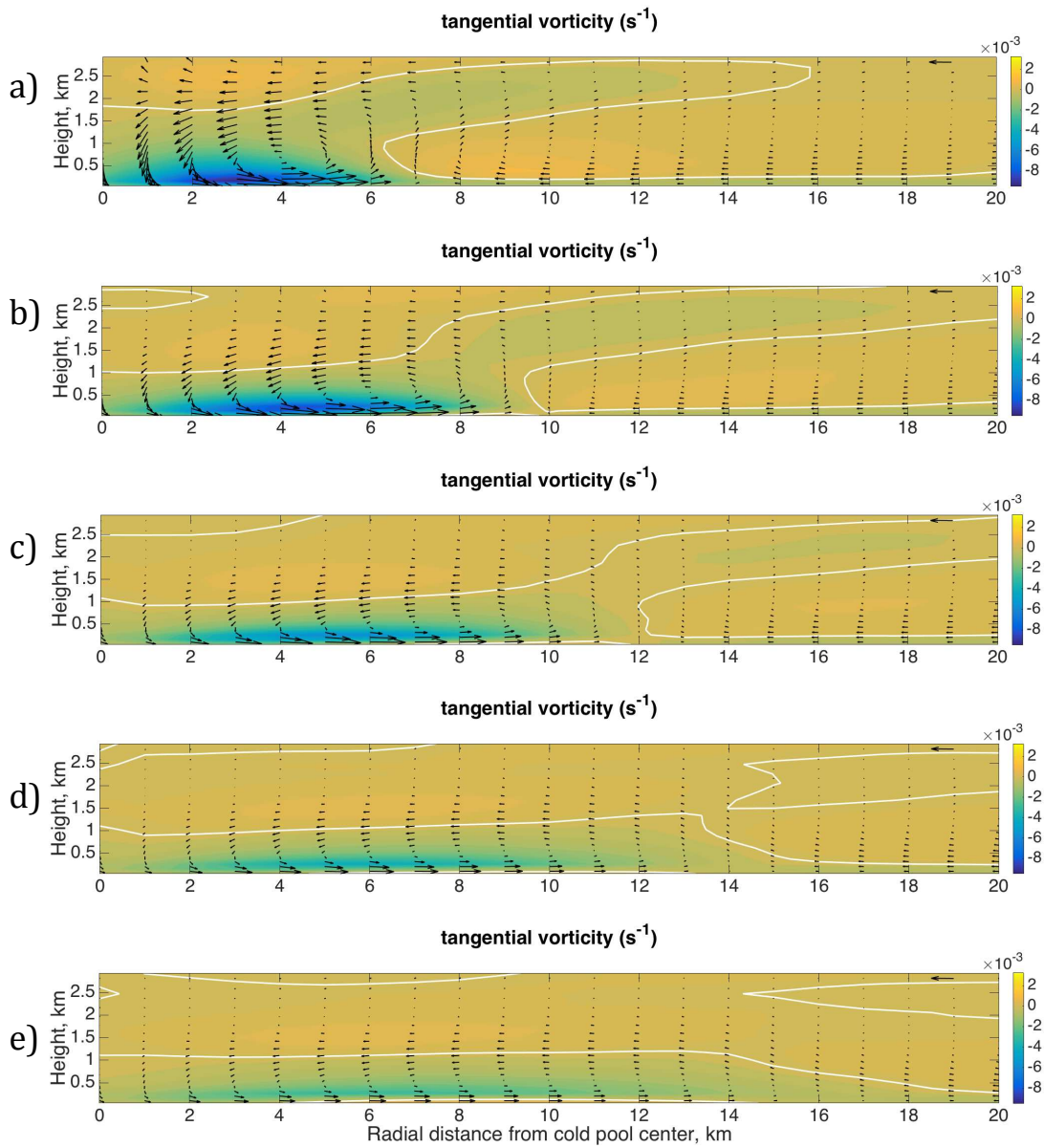


Figure 2.20. Composites of tangential vorticity (colors) and transverse circulation (arrows) at (a)  $t = 0$  minutes, (b)  $t = 15$  minutes, (c)  $t = 30$  minutes, (d)  $t = 45$  minutes, and (e)  $t = 60$  minutes. The leftward-pointing arrow in the upper-right corner has a magnitude of  $1 \text{ m s}^{-1}$ . The zero-contour of tangential vorticity is plotted in white.

## CHAPTER 3: SOIL MOISTURE DEPENDENCE

### 3.1 Introduction

Convective cold pools are regions of evaporatively-cooled air that form within the boundary layer in association with convective precipitating systems. The cold pool formation process is initiated when evaporative cooling and hydrometeor loading combine to create a region of locally dense air [e.g., *Srivastava, 1987; Torri and Kuang, 2016*]. The air's negative buoyancy propels it downward to form a convective-scale downdraft that penetrates the boundary layer to reach the surface. Upon reaching the surface, the downdraft air spreads out laterally, displacing lower-density boundary layer air. The dense air that collects near the surface is the convective cold pool. In addition to locally cooler air, convective cold pools are associated with gusty winds. The lateral expansion of convective cold pools is driven by density current dynamics, such that the gust front that bounds the cold pool propagates with a speed that depends on the difference in density between the cold pool air and the ambient boundary layer air [e.g., *Charba, 1974*]. The propagating gust front may trigger new convection by lifting boundary layer air to its level of free convection [e.g., *Moncrieff and Liu, 1999; Torri et al., 2015*].

Despite their importance for convective organization, convective cold pools are not well-represented in most climate models, and several aspects of cold pool development are not well-understood. One active area of research is the importance of surface sensible and latent heat fluxes on cold pool evolution and dissipation [*Ross et al., 2004; Gentine et al., 2016; Grant and van den Heever, 2016*].

Surface fluxes depend not only on atmospheric properties such as wind and specific humidity, but also on the characteristics of the land and/or ocean surface beneath. By affecting

surface fluxes, surface characteristics may influence cold pool structure and evolution. For instance, under some conditions cold pools have been found to generate “rings” of enhanced atmospheric water vapor [e.g., *Tompkins, 2001; Langhans and Romps, 2015; Schlemmer and Hohenegger, 2016*]. *Schlemmer and Hohenegger [2016]* modeled this phenomenon both over land and over ocean and found that the partitioning of contributions from various moisture sources was different over land than over ocean. Recent work by *Gentine et al. [2016]* and *Grant and van den Heever [2016]* has also emphasized the importance of interactive surface heat fluxes in correctly representing cold pools in numerical simulations.

Of interest in this study is the influence of soil moisture on the characteristics and evolution of convective cold pools. Three idealized simulations of afternoon convection are performed, each initialized with a different amount of soil moisture. Soil moisture may influence surface fluxes in multiple ways. As soil moisture increases, more moisture becomes available to evaporate during the day, and plants will transpire more water vapor as they become less stressed and open their stomata [*Fisher et al., 2006*]. Therefore, surface latent heat fluxes can be expected to increase with increasing soil moisture. As soil moisture decreases, decreased specific heat capacity of the soil system and decreased evaporative cooling combine to allow increased daytime heating of the soil and thus greater surface sensible heat fluxes.

These changes in surface fluxes may affect cold pools not only directly through effects on cold pool air during the cold pool life cycle, but also indirectly through effects on the environment in which cold pools form. Over the course of the day, increased surface latent heat fluxes from moister soil yield increased boundary layer humidity, which decreases the potential for precipitation to evaporate as it falls through the boundary layer. Increased daytime heating of drier soil, on the other hand, can yield decreased boundary layer relative humidity and more

vigorous boundary layer circulations. Decreased boundary layer relative humidity will promote evaporation of precipitation falling through the boundary layer and will thus promote evaporative cooling. More vigorous boundary layer circulations may promote the development of convection, as well as the entrainment of environmental air into a developing cold pool, thus hastening the cold pool's dissipation [*Grant and van den Heever, 2016*].

The goal of this work is to investigate the effects of soil moisture on convective cold pool development in a set of high-resolution numerical model simulations. Three simulations are performed, each with a different initial soil moisture content. A cold pool identification algorithm is applied in order to generate a composite of the cold pools in each simulation. The differences between the composites are then explored, and physical mechanisms are assessed. The rest of this chapter is structured as follows: Section 3.2 discusses the model setup and the simulations that were performed. In Section 3.3, the results are presented, and in Section 3.4, the results are discussed in the context of convective organization. Finally, Section 3.5 concludes the paper.

### **3.2 Model Setup**

The simulations used in this study were performed using the open-source Regional Atmospheric Modeling System (RAMS) (<http://reef.atmos.colostate.edu/~sue/vdhp/rams.php>) [*Cotton et al., 2003; Saleeby and van den Heever, 2013*]. RAMS is a regional, non-hydrostatic model and is coupled to the Land-Ecosystem-Atmosphere Feedback (LEAF) version 3 land surface model [*Walko et al., 2000*].

This study uses a subset of the idealized tropical sea-breeze simulations conducted by *Grant and van den Heever* [2014, hereafter GvdH14]. The simulations are conducted on a non-rotating domain whose meridional extent is 200 km and whose zonal extent is 550 km. The

domain's lateral boundary conditions are periodic in the meridional and open-radiative [Klemp and Wilhelmson, 1978] in the zonal. The domain's western third has an ocean surface and whose eastern two-thirds has a tropical rainforest-type surface. The simulations are run at a horizontal grid spacing of 1 km and 57 stretched vertical levels whose spacing varies from 100 m near the surface to 1 km aloft. The simulations are initialized at 700 LT and run for 16 hours.

The simulations of interest are the CTL, s50, and s25 simulations of GvdH14, which are initialized with 75%, 50%, and 25% soil moisture saturation ( $0.315 \text{ m}^3 \text{ m}^{-3}$ ,  $0.21 \text{ m}^3 \text{ m}^{-3}$ , and  $0.105 \text{ m}^3 \text{ m}^{-3}$  soil moisture content), respectively. In this study these will be referred to as the MOIST, MID, and DRY simulations. Although these simulations were originally conducted to assess the impacts of soil moisture on sea-breeze convection, in this study the focus is on the convection that occurs ahead of the sea-breeze front. The location of the sea-breeze front is identified according to the methods in GvdH14, and the analyses are limited to the part of the domain extending eastward from the zonal location of the sea-breeze front to 50 km from the eastern edge of the domain (to avoid contamination from the eastern open-radiative boundary, as in GvdH14). The reader is referred to GvdH14 and references contained therein for additional details regarding RAMS and the model setup.

### 3.3 Results

Composites are generated from cold pools identified during the 160-minute period from 14:15–16:55 LT according to the methods set forth in *Drager and van den Heever* [2016, hereafter DvdH16]. This time period is chosen because it represents a time during which the simulation has already spun up, and multiple rounds of convection have already occurred. During this time period, 207, 205, and 222 cold pools are identified in the MOIST, MID, and DRY simulations, respectively. In the discussion on the composites that follows, time  $t = 0$  is

defined as the time at which each cold pool is identified. This time corresponds to the early part of the cold pool lifecycle [DvdH16].

It should be noted that the near-surface values of density potential temperature  $\theta_\rho$  [Emanuel, 1994] are approximately 2 K higher in the DRY simulation than in the MOIST and MID simulations, whose near-surface values of  $\theta_\rho$  differ from each other by approximately 0.25 K (not shown). When the soil moisture is reduced, insolation is able to raise the temperature of the soil more efficiently because there is less water to evaporate and hence more energy goes into raising the soil temperature. Due to nonlinear land-surface-ecosystem processes, the effects of reduced soil moisture are much more pronounced in the DRY simulation than in the MID simulation, despite the fact that soil moisture varies linearly (25%, 50%, and 75% of saturation) between the simulations at the time of initialization. Thus, the DRY simulation experiences the most surface heating. Due to the enhanced daytime heating, the boundary layer is also deeper in the DRY simulation than in the MOIST and MID simulations (not shown). The cloud base is also higher (not shown).

Figure 3.1 shows radial profiles for several surface and near-surface variables at  $t = -30$  minutes, before cold pool formation. Figure 3.1a shows the near-surface buoyancy, calculated as in GvdH14. In all three simulations, buoyancy is positive in the center (i.e., in the region in which the cold pool will eventually form). The largest buoyancy perturbation is observed in the DRY simulation. The positive buoyancy anomaly is accompanied by a positive water vapor perturbation in the MOIST and MID simulations but not in the DRY simulation (Figure 3.1b). The ambient near-surface water vapor is also much lower in the DRY simulation than in the MOIST and MID simulations. The ambient near-surface equivalent potential temperature  $\theta_e$  (Figure 3.1c) is also therefore lower in the DRY simulation despite the greater temperatures. The

velocity fields contain the signature of inflow into the parent clouds that will eventually spawn the cold pools, with negative radial velocity surrounding the center (Figure 3.1e) and positive near-surface vertical velocity at the center (Figure 3.1d). A low-pressure anomaly near the center is evident in all three simulations (Figure 3.1f), another signature of the convection that is about to give rise to the development of the convective cold pools.

Figure 3.2 shows radial profiles for the same variables at  $t = 0$  minutes, the time at which cold pools are first detected. It is evident from these profiles that the cold pools are stronger in the DRY simulation than in the MOIST and MID simulations. The near-center buoyancy depression is slightly—but statistically significantly—larger in the DRY simulation (Figure 3.2a), as are the downward motion (Figure 3.2d) and the radial wind outflow (Figure 3.2e). The positive pressure perturbation is also stronger in the DRY simulation than in the MOIST and MID simulations. The subcloud layer in the DRY simulation is deeper and drier than that in the MOIST and MID simulations. Thus, there is greater opportunity for precipitation to evaporate and cool the subcloud layer as it descends through the column, and the result is a deeper (as confirmed by the greater surface pressure perturbation), stronger cold pool.

One notable difference in cold pool structure between the simulations is that whereas the MOIST and MID simulations exhibit the water vapor “rings” documented in previous studies [e.g., *Tompkins, 2001; Langhans and Romps, 2015; Schlemmer and Hohenegger, 2016*], the DRY simulation does not (Figure 3.2b). Instead, the DRY simulation exhibits a positive water vapor perturbation near the center. Since there is no dry perturbation near the center, the signature equivalent potential temperature ( $\theta_e$ ) depression of the cold pools in the water vapor field is diminished in the DRY simulation (Figure 3.2c). Indeed, even though the DRY

simulation has the strongest cold pools in terms of buoyancy and wind field characteristics, it has the weakest cold pools in terms of  $\theta_e$ .

The different cold pool water vapor structures can be explained in part by the latent heat fluxes (Figure 3.2h), which were found by *Langhans and Romps* [2015] to be the primary contributor to water vapor rings. In all three simulations, latent heat fluxes take on a ring-like structure. Near the cold pool center, latent heating is suppressed by weak winds and shading by the cold pool's parent cloud. Adjacent to the center, winds are stronger, and thus latent heating is enhanced. However, latent heating can only be enhanced where soil moisture is available for evapotranspiration. Precipitation does fall in the center of the cold pool (Figure 3.2i), and this precipitation is available in all three simulations to be evaporated. However, away from the region into which precipitation has fallen, the latent heat fluxes in the DRY simulation are generally suppressed due to the relative lack of available soil moisture for evapotranspiration.

This explains why the outer water vapor rings do not form in the DRY simulation but does not explain why the inner dry region does not form. The inner dry region forms due to the injection of dry air into the cold pool from aloft. However, the downward transport of dry air from aloft is accompanied by precipitation, which may evaporate into this initially dry air. The water vapor content of the lower levels is initially quite different between the simulations (Figure 3.1b), with much greater near-surface water vapor in the MOIST and MID simulations than in the DRY simulation. The dry air from aloft, when modified by the evaporation of precipitation and injected into the boundary layer, is moister than the ambient air in the DRY simulation but drier than the ambient air in the MOIST and MID simulations.

Also apparent from Figure 3.2 is that the cold pools in the DRY simulation are smaller than those in the MOIST and MID simulations. This difference is subtle but can be seen in the

location of the zero-crossings of the respective vertical velocity curves in Figure 3.2d. If the location of the zero-crossing of  $\frac{\partial^2 \theta_p}{\partial r^2}$  (not shown; see DvdH16) can be taken to be the composite cold pool radius, then the DRY composite cold pool radius is approximately 3.5 km, whereas the MOIST composite cold pool radius is approximately 3.9 km, representing a difference in cold pool area of ~25%. There is an apparent contradiction here. According to density current theory [e.g., *Benjamin*, 1968], a denser (more negatively buoyant) cold pool should expand more rapidly than should one that is less negatively buoyant. Indeed, the radial outflow is stronger in the DRY case than in the MOIST and MID cases (Figure 3.2e). The resolution of this apparent contradiction lies in the sensible heat fluxes (Figure 3.2g). Sensible heat fluxes weaken the cold pool by warming the cold pool air, and the DRY simulation exhibits much greater sensible heat fluxes relative to the MOIST and MID simulations. Thus, even though cold pool air in the DRY simulation initially has a stronger negative buoyancy perturbation and initially flows outward more quickly, the density current flow is stemmed by substantial heating from sensible heat fluxes, and the resulting cold pools are thus smaller than those in the MOIST and MID simulations.

Figure 3.3 shows the various radial profiles at  $t = 60$  minutes, one hour after the cold pools are identified. At this point, cold pool dissipation is underway, and the negative buoyancy anomalies (Figure 3.3a) are smaller than in Figure 3.2. There is also negative buoyancy away from the cold pool center; this is associated with contamination from the sea-breeze front. In all three simulations, particularly the DRY simulation, there is now enhanced water vapor near the cold pool center (Figure 3.3b). This enhanced water vapor is associated with the moist patch that forms when precipitation soaks the ground beneath the cold pool, resulting in enhanced latent

heat fluxes (Figure 3.3h) and negative sensible heat fluxes (Figure 3.3g) (see DvdH16 for more discussion of this feature).

One interesting result at this time is that the radial outflow (Figure 3.3e) at radius  $r \sim 10$ – $15$  km is greater in the MOIST simulation than in the other two. This result is not statistically significant at  $t = 60$  minutes but does become statistically significant at the 95% level at  $t = 70$  minutes (not shown). Since the sensible heat fluxes are weakest in the MOIST simulation, the density current outflow is able to survive longer without dissipating.

### **3.4 Discussion**

These results have implications for the organization of future convection within the simulations. As was observed in Figure 3.1, new convection preferentially forms in regions of enhanced water vapor in the MOIST and MID simulations. When water vapor rings are present, this then means that new convection can preferentially form along the edges of existing cold pools. Indeed, water vapor rings are present in the MOIST and MID simulations. However, the lack of water vapor rings in the DRY simulation implies potentially a different form of convective organization. It is still possible that subsequent convection forms on the periphery of cold pools in the DRY simulation. In the DRY simulation, convection may form along the edges of existing cold pools not because there is a positive water vapor anomaly but because of the lifting provided by the gust front. However, in this case, the convection is not associated with a positive water vapor anomaly. And if convection is suppressed in the centers of cold pools due to the temperature depressions there, then cold pool edges may be the only locations available for new convection to form.

### 3.5 Summary and Conclusions

Convective cold pools have important implications for convective organization. However, it is not well understood how the properties of convective cold pools vary as a function of their environment. This study has examined the differences in cold pool properties between simulations initialized with different amounts of soil moisture. These differences are summarized in Figure 3.4. It was found that the DRY simulation exhibited the strongest cold pools, with the largest negative buoyancy perturbations and the strongest radial outflow. However, despite having cold pools with the strongest radial outflows, the DRY simulation also had the smallest cold pools. This is due to the presence of the strongest sensible heat fluxes that caused the density currents to dissipate as they spread out. The structure of the cold pools' water vapor fields also differed between simulations. Water vapor "rings" appear in the MOIST and MID simulations but not in the DRY simulation. These differences in cold pool structure have implications for the locations and mechanisms by which new convection may form.

We have seen here the substantial impact that a change in soil moisture can have on cold pool properties. Cold pools are shaped by their environments, and these results serve to emphasize the importance of considering environmental characteristics both when representing cold pools in simulations and when analyzing the role of convective cold pools in the atmosphere.

### 3.6 Figures

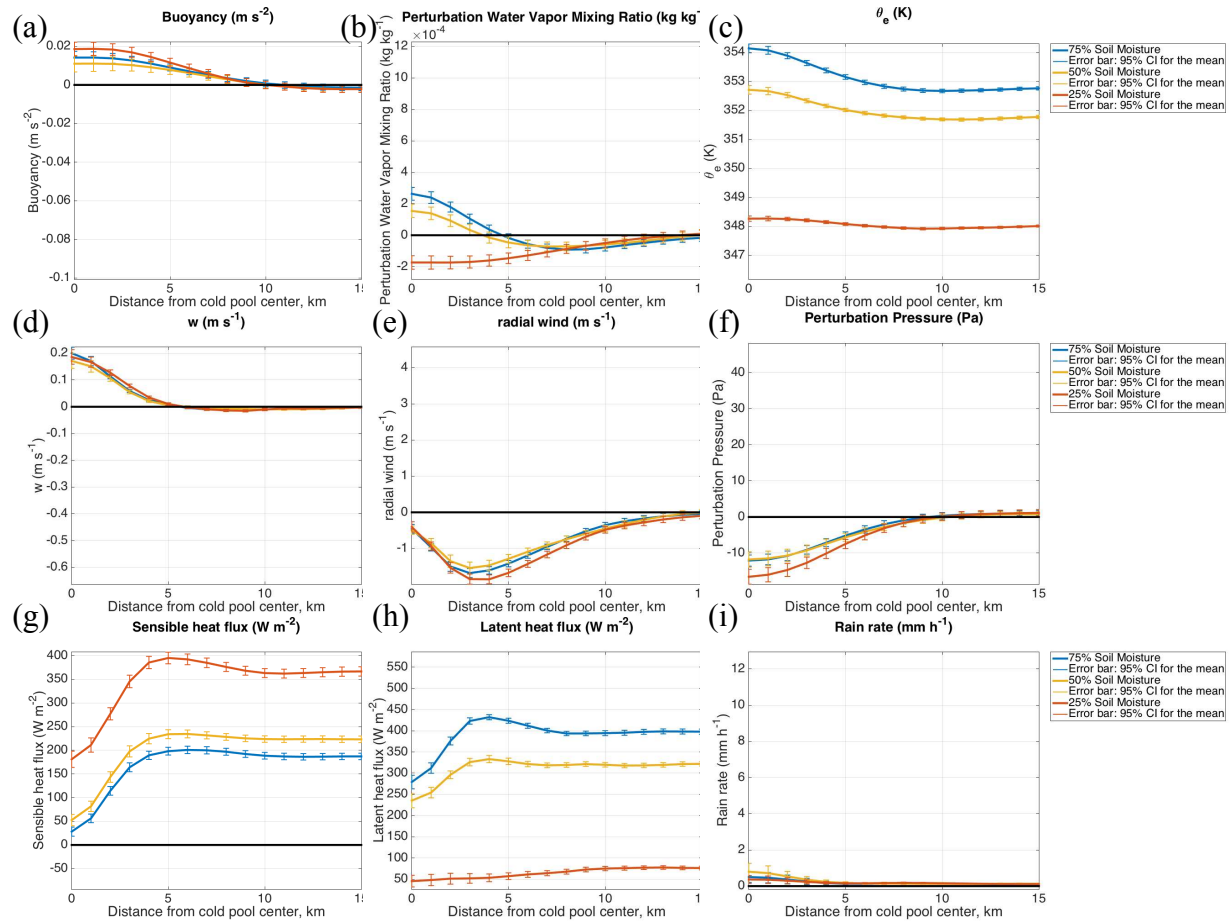


Figure 3.1. Surface and near-surface variables at  $t = -30$  minutes: (a) buoyancy, (b) perturbation water vapor mixing ratio  $r'_v$ , (c) equivalent potential temperature  $\theta_e$ , (d) vertical velocity  $w$ , (e) radial wind  $v_r$ , (f) perturbation pressure  $p'$ , (g) surface sensible heat flux, (h) surface latent heat flux, and (i) surface rain rate. Variables (a) through (f) are at height  $z \sim 50$  m, with the exception of (d), which is at  $z = 100$  m. Error bars indicate the 95% confidence interval for the mean.

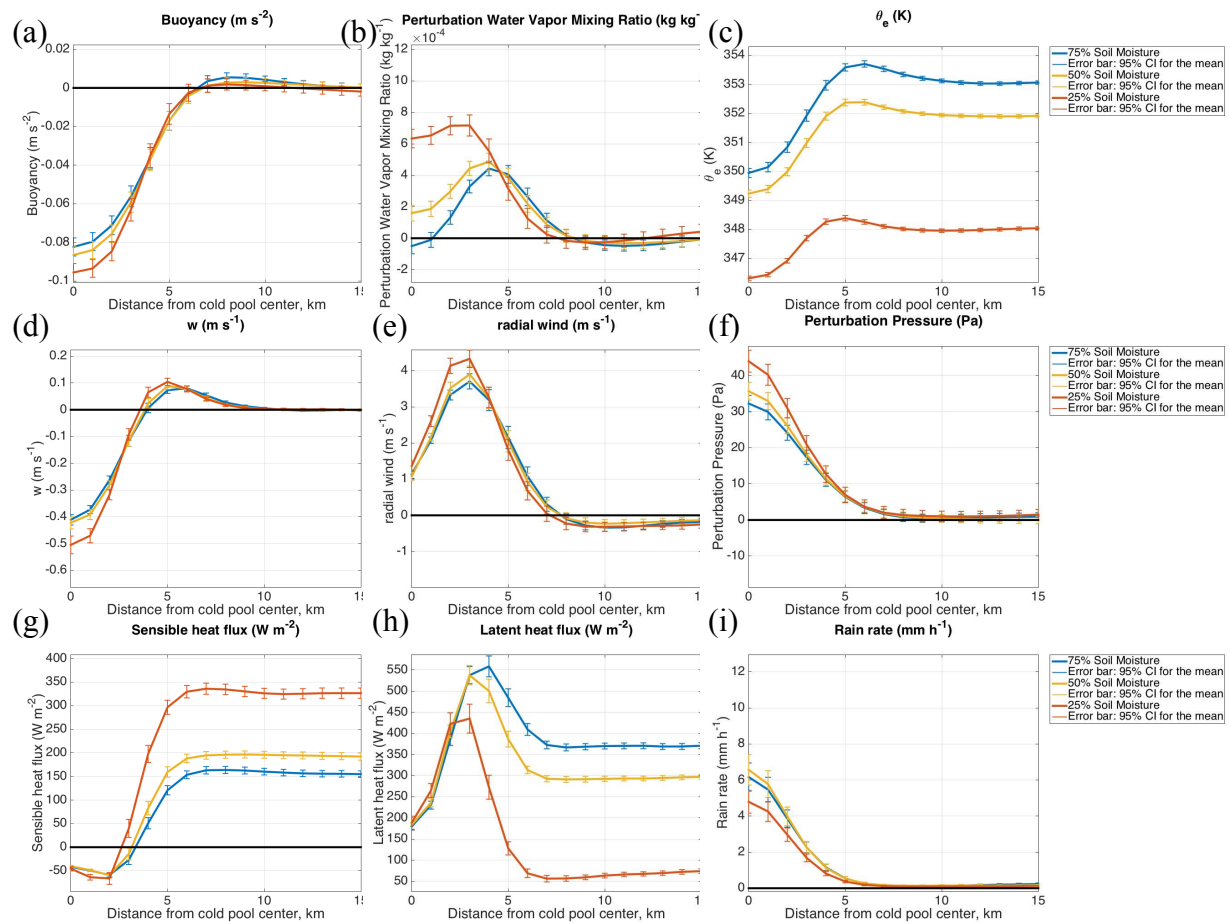


Figure 3.2. Surface and near-surface variables at  $t = 0$  minutes.

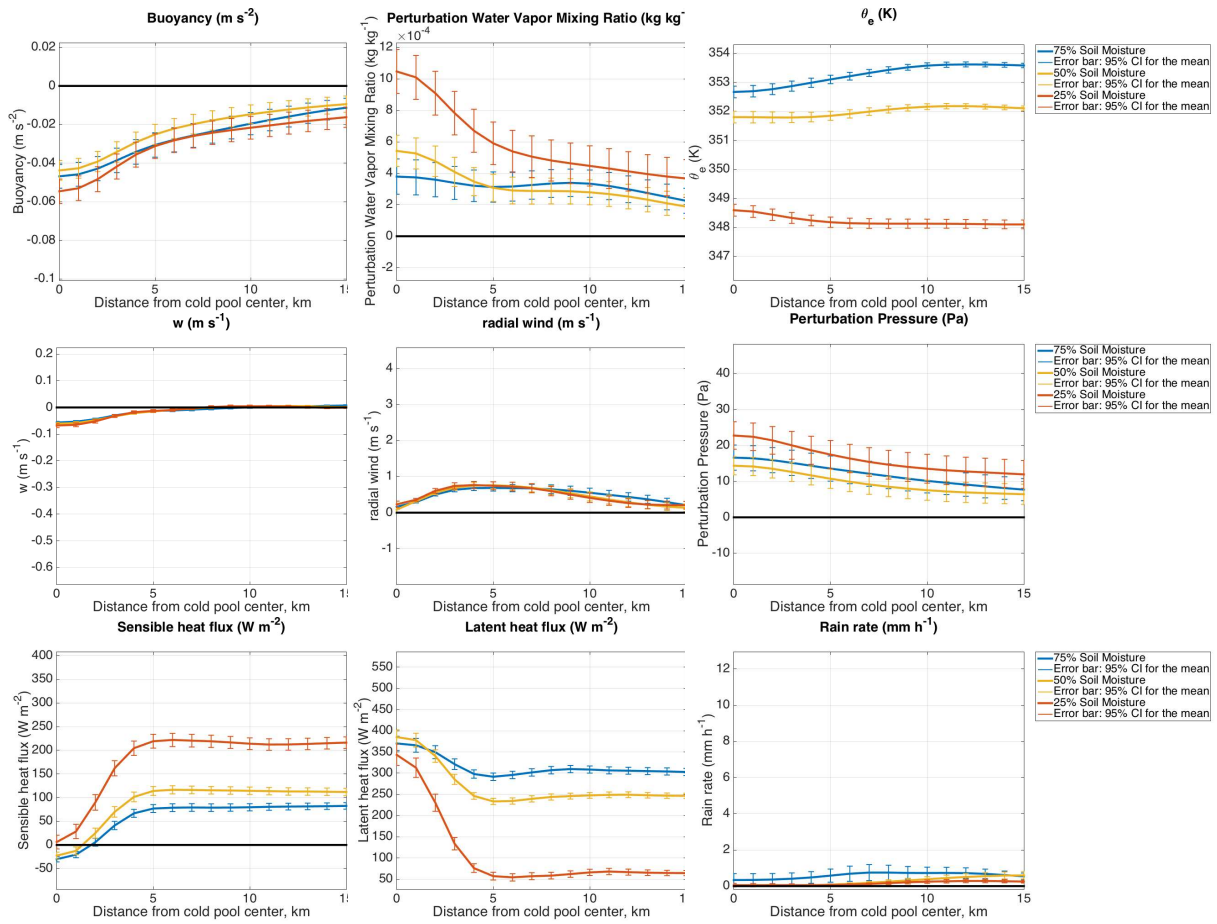


Figure 3.3. Surface and near-surface variables at  $t = 60$  minutes.

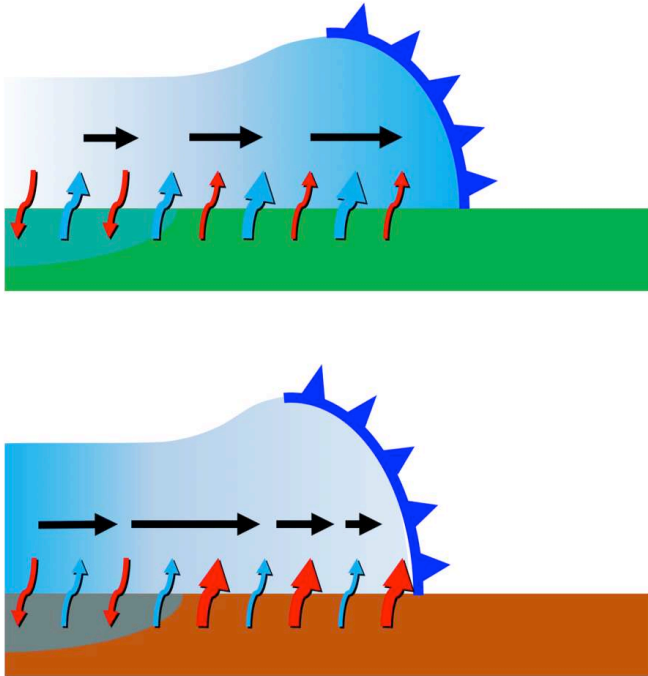


Figure 3.4. Summary schematic of the differences between cold pools in the MOIST (top) and DRY (bottom) simulations. The schematic is a vertical cross-section, with the center of the cold pool at left. Black arrows indicate winds, blue arrows indicate surface latent heat fluxes, and red arrows indicate surface sensible heat fluxes. Blue shading above ground indicates enhanced water vapor relative to surroundings, and blue shading below ground indicates wet soil associated with the moist patch.

## CHAPTER 4: CONCLUDING REMARKS

### 4.1 Main Conclusions

Convective cold pools play an important role in Earth's climate system. The research outlined in this thesis contributes to our understanding of convective cold pools through the development of a new algorithm for identifying and tracking cold pools (Chapter 2), and through the application of this algorithm to investigate the effects of soil moisture changes on cold pool development (Chapter 3).

Chapter 2 began with a review of existing methods for identifying convective cold pools in observations and in models. The strengths and weaknesses of various variables for cold pool identification were then assessed. None of the assessed variables met all of the criteria that were set forth for simple threshold-based cold pool identification, and so a new identification method was developed that relied on the second radial derivatives of model variables rather than simple thresholding of the raw variables themselves. Specifically, this new method involved calculating the second radial derivative of density potential temperature,  $\frac{\partial^2 \theta_\rho}{\partial r^2}$ , and taking the boundary of the convective cold pool to be the contour at which  $\frac{\partial^2 \theta_\rho}{\partial r^2} = 0$ . The resulting cold pool boundary tended to be located in the regions in which the gradient of density potential temperature is greatest, and thus the boundary tended to be in a suitable location. This method was shown to succeed across a variety of convective cold pools in the simulation being analyzed and was also shown to be able to determine the boundaries of colliding cold pools, representing an improvement on previous approaches.

The cold pool identification algorithm was applied to a simulation of sea-breeze convection, and cold pools ahead of the sea breeze were averaged together to form a composite

cold pool. Several findings were in agreement with existing knowledge of convective cold pools. Cold pools were found to form preferentially in areas with enhanced values of  $\theta_p$  and  $r_v$  with winds directed inward toward the location in which the cold pool would eventually form. The cold pool exhibited  $\theta_p$  values approximately 2 to 3 K cooler than environmental values, on average, and the  $r_v$  field was observed to exhibit rings of enhanced moisture along the cold pool periphery. In the kinematic fields, cold pools exhibited radial wind speeds, on average, of 3 to 4  $\text{m s}^{-1}$ , and cold pools were found to consist of a region of downdrafts surrounded by a ring of updrafts. These results confirmed the viability and reliability of the cold pool identification algorithm.

One novel result arising from this research is the identification of what is termed a *moist patch* in the parts of cold pools in which the ground was soaked by rainwater. These moist patches occupy only a small fraction of cold pools since cold pools themselves occupy much more area than experiences rain. Within the moist patches, values of  $\theta_p$  are lower than in the rest of the cold pool, which recovers to background environmental temperatures more quickly. Furthermore, values of  $r_v$  are higher within the moist patch. Sensible heat fluxes are negative since the rainwater cools the surface to below the ambient air temperature, and latent heat fluxes are enhanced due to the presence of additional ground moisture. It is speculated that the role of the moist patch is to delay the recovery of the interior of the cold pool and to further prevent the development of new convection within cold pool interiors.

In Chapter 3, three simulations of tropical sea-breeze convection were analyzed. These simulations differed in their initial soil moisture content and were referred to as the MOIST, MID, and DRY simulations. For each simulation, the cold pool identification algorithm developed in Chapter 2 was applied, and a composite cold pool was generated. It was found that

the MOIST and MID simulations behaved similarly to one another, whereas the DRY simulation behaved much differently, as was observed for non-cold pool-related trends in Grant and van den Heever (2014). The DRY simulation was observed to have the strongest cold pools, with colder  $\theta_p$  perturbations relative to the environmental value and more vigorous radial wind outflow and vertical motions. Despite having the strongest radial wind outflow, the DRY simulation was observed to have the smallest convective cold pools. This result was attributed to the greater surface sensible heat fluxes in the DRY simulation compared to the other two simulations. The sensible heat fluxes caused the cold pools in the DRY simulation to dissipate as they expanded, and therefore prevented the cold pools in the DRY simulation from achieving the sizes of their counterparts in the MOIST and MID simulations.

It was also found that whereas the cold pools in the MOIST and MID simulations exhibited the rings of enhanced water vapor observed in Chapter 2 and in past studies of tropical convective cold pools, cold pools in the DRY simulation exhibited no rings of enhanced water vapor, and instead exhibited enhanced water vapor near their centers. This difference was attributed to several mechanisms. Firstly, the ambient near-surface water vapor was higher in the MOIST and MID simulations and lower in the DRY simulation. This created a scenario in which the evaporation-modified downdraft air entering the cold pool was moister than the ambient air in the DRY simulation but drier than the ambient air in the MOIST and MID simulations. Thus, the cold pool interiors were moister than their surroundings in the DRY simulation and drier than their surroundings in the MOIST and MID simulations. Secondly, the moisture rings themselves form in large part due to surface latent heat fluxes [*Langhans and Romps, 2015*]. In the DRY simulation, the relative lack of water available for evapotranspiration suppressed the surface latent heat fluxes, and the rings of enhanced water vapor did not form. The implication for future

convection was that whereas convection in the MOIST and MID simulations could form along the moisture rings and thus form in regions of both enhanced  $\theta_\rho$  and enhanced  $r_v$ , convection in the DRY simulation would form within regions of enhanced  $\theta_\rho$  only.

The analysis performed in Chapter 3 demonstrates the utility of the cold pool identification algorithm developed in Chapter 2 and also highlights the effect that a change in a single environmental parameter—soil moisture—can have on convective cold pool evolution. The analyses performed in Chapters 2 and 3 as a whole emphasize the value of high-resolution numerical model simulations for furthering our understanding of convective cold pools and of atmospheric convection in general.

## 4.2 Future Work

### 4.2.1 Algorithm Development

Although the cold pool identification algorithm performs well on the simulations tested, it remains to be seen how well it will perform in other settings, such as squall line simulations, supercell simulations, and large-domain simulations of tropical convection in radiative-convective equilibrium, as well as at different resolutions. One limitation of the analysis method used here is the assumption during the compositing stage that cold pools are stationary; this assumption does not necessarily hold in other settings, particularly in the mid-latitudes, where vertical wind shear plays an important role. One solution would be to track convective cold pools over time and allow their centroids to move. To some extent this is already done during the algorithm's tracking stage, but due to the algorithm design it is currently impossible to continue tracking convective cold pools beyond 10 minutes following the dissipation of the parent precipitation system. Even when convective cold pools are stationary, the  $\frac{\partial^2 \theta_\rho}{\partial r^2} = 0$  contour eventually ceases to yield smooth boundaries and in some cases becomes wrapped around the

boundary of the moist patch instead of the boundary of the broader cold pool. It might be possible to overcome this problem through the deployment of more sophisticated techniques, such as an active contours algorithm [e.g., *Caselles et al.*, 1997; *Chan and Vese*, 2001] or optical flow [e.g., *Horn and Schunck*, 1981].

Another area for additional algorithm development is the determination of convective cold pool depth. Convective cold pools exist in three spatial dimensions, whereas the existing algorithm analyzes them without regard for the vertical spatial dimension. Unfortunately, as discussed in Chapter 2, the definition of convective cold pool depth is significantly more difficult than the definition of horizontal extent due to the lack of sharp vertical gradients in model fields. One possible approach to defining cold pool vertical extent would be to assess the depth over which the radial velocity component is positive. However, further work would need to be done to ensure such an approach has a true physical basis and yields reasonable theoretical cold pool propagation speeds. Another approach, which would yield a uniform depth for the cold pool, would be to examine the  $\frac{\partial^2 \theta_p}{\partial r^2} = 0$  contour at each vertical level, and to determine the height at which this curve is no longer sufficiently circular or well-defined.

#### 4.2.2 Further Cold Pool Studies

The study performed in Chapter 3 is just one example of the type of investigation that can be carried out using the algorithm developed in Chapter 2. Recall that the sea-breeze simulations of *Grant and van den Heever* [2014] were conducted with several types of perturbations. In addition to soil moisture, *Grant and van den Heever* [2014] also investigated the effects of variations in surface roughness and atmospheric aerosol concentration on the development of the sea breeze and sea-breeze convection. It would be straightforward to apply the methods of Chapter 3 to these additional simulations and investigate the effects of surface roughness and

atmospheric aerosol concentrations, as well as synergistic effects, on convective cold pool development.

It would also be interesting to apply the cold pool identification algorithm to different types of settings. For instance, the algorithm might be applied to large-domain simulations of tropical, oceanic convection in radiative-convective equilibrium in order to assess how cold pool statistics change under different scenarios, e.g., different sea-surface temperatures or different types of radiative forcing (constant vs. diurnal cycle).

Ultimately, the cold pool identification algorithm is a useful tool that can be deployed in the future to further our understanding of convective cold pools and of convective processes as a whole.

## REFERENCES

- Addis, R. P., M. Garstang, and G. D. Emmitt (1984), Downdrafts from Tropical Oceanic Cumuli, *Boundary-Layer Meteorol.*, 28(1), 23–49, doi:10.1007/BF00119455.
- American Meteorological Society (2016a), Cold Pool, *Gloss. Meteorol.*
- American Meteorological Society (2016b), Wake, *Gloss. Meteorol.*
- Barnes, G. M., and M. Garstang (1982), Subcloud Layer Energetics of Precipitating Convection, *Mon. Weather Rev.*, 110(2), 102–117, doi:10.1175/1520-0493(1982)110<0102:SLEOPC>2.0.CO;2.
- Benjamin, T. B. (1968), Gravity currents and related phenomena, *J. Fluid Mech.*, 31(02), 209, doi:10.1017/S0022112068000133.
- Bryan, G. H., and M. D. Parker (2010), Observations of a Squall Line and Its Near Environment Using High-Frequency Rawinsonde Launches during VORTEX2, *Mon. Weather Rev.*, 138(11), 4076–4097, doi:10.1175/2010MWR3359.1.
- Byers, H. R., and R. R. Braham (1949), *The Thunderstorm: Final Report of the Thunderstorm Project*, U.S. Gov. Printing Off., Washington, D. C.
- Caesar, K.-A. L. (1995), Cold Domes Over the Warm Pool: A Study of the Properties of Cold Domes Produced by Mesoscale Convective Systems During TOGA COARE, Texas A&M University.
- Caselles, V., R. Kimmel, and G. Sapiro (1997), Geodesic Active Contours, *Int. J. Comput. Vis.*, 22(1), 61–79, doi:10.1023/A:1007979827043.
- Chan, T. F., and L. A. Vese (2001), Active contours without edges, *IEEE Trans. Image Process.*, 10(2), 266–277, doi:10.1109/83.902291.

- Charba, J. (1974), Application of Gravity Current Model to Analysis of Squall-Line Gust Front, *Mon. Weather Rev.*, *102*(2), 140–156, doi:10.1175/1520-0493(1974)102<0140:AOGCMT>2.0.CO;2.
- Cotton, W. R. et al. (2003), RAMS 2001: Current status and future directions, *Meteorol. Atmos. Phys.*, *82*(1), 5–29, doi:10.1007/s00703-001-0584-9.
- Dawson, D. T., M. Xue, J. A. Milbrandt, and M. K. Yau (2010), Comparison of Evaporation and Cold Pool Development between Single-Moment and Multimoment Bulk Microphysics Schemes in Idealized Simulations of Tornadic Thunderstorms, *Mon. Weather Rev.*, *138*(4), 1152–1171, doi:10.1175/2009MWR2956.1.
- Del Genio, A. D., J. Wu, and Y. Chen (2012), Characteristics of mesoscale organization in WRF simulations of convection during TWP-ICE, *J. Clim.*, *25*(17), 5666–5688, doi:10.1175/JCLI-D-11-00422.1.
- DeMott, P. J., A. J. Prenni, X. Liu, S. M. Kreidenweis, M. D. Petters, C. H. Twohy, M. S. Richardson, T. Eidhammer, and D. C. Rogers (2010), Predicting global atmospheric ice nuclei distributions and their impacts on climate, *Proc. Natl. Acad. Sci. U. S. A.*, *107*(25), 11217–22, doi:10.1073/pnas.0910818107.
- Doswell, C. A. (1987), The Distinction between Large-Scale and Mesoscale Contribution to Severe Convection: A Case Study Example, *Weather Forecast.*, *2*(1), 3–16, doi:10.1175/1520-0434(1987)002<0003:TDBLSA>2.0.CO;2.
- Doswell, C. A., and P. M. Markowski (2004), Is Buoyancy a Relative Quantity?, *Mon. Weather Rev.*, *132*(4), 853–863, doi:10.1175/1520-0493(2004)132<0853:IBARQ>2.0.CO;2.
- Drager, A. J., and S. C. van den Heever (2016), Characterizing Convective Cold Pools, in prep. for *J. Adv. Model. Earth Syst.*

- Droegemeier, K. K., and R. B. Wilhelmson (1987), Numerical Simulation of Thunderstorm Outflow Dynamics. Part I: Outflow Sensitivity Experiments and Turbulence Dynamics, *J. Atmos. Sci.*, *44*(8), 1180–1210, doi:10.1175/1520-0469(1987)044<1180:NSOTOD>2.0.CO;2.
- Emanuel, K. A. (1994), *Atmospheric Convection*, Oxford University Press, New York.
- Engerer, N. A., D. J. Stensrud, and M. C. Coniglio (2008), Surface Characteristics of Observed Cold Pools, *Mon. Weather Rev.*, *136*(12), 4839–4849, doi:10.1175/2008MWR2528.1.
- Feng, Z., S. Hagos, A. K. Rowe, C. D. Burleyson, M. N. Martini, and S. P. de Szoeke (2015), Mechanisms of convective cloud organization by cold pools over tropical warm ocean during the AMIE/DYNAMO field campaign, *J. Adv. Model. Earth Syst.*, *357–381*, doi:10.1002/2014MS000384.
- Fisher, R. A., M. Williams, R. L. Do Vale, A. L. Da Costa, and P. Meir (2006), Evidence from Amazonian forests is consistent with isohydric control of leaf water potential, *Plant, Cell Environ.*, *29*(2), 151–165, doi:10.1111/j.1365-3040.2005.01407.x.
- Gaynor, J. E., and C. F. Ropelewski (1979), Analysis of the convectively modified GATE boundary layer using in situ and acoustic sounder data, *Mon. Weather Rev.*, *107*, 985–993, doi:10.1175/1520-0493(1979)107<0985:AOTCMG>2.0.CO;2.
- Geldmeier, M. F., and G. M. Barnes (1997), The “Footprint” under a Decaying Tropical Mesoscale Convective System, *Mon. Weather Rev.*, *125*(11), 2879–2895, doi:10.1175/1520-0493(1997)125<2879:TFUADT>2.0.CO;2.
- Gentine, P., A. Garelli, S. B. Park, J. Nie, G. Torri, and Z. Kuang (2016), Role of surface heat fluxes underneath cold pools, *Geophys. Res. Lett.*, *43*(2), 874–883, doi:10.1002/2015GL067262.

- Goff, R. C. (1976), Vertical Structure of Thunderstorm Outflows, *Mon. Weather Rev.*, *104*(11), 1429–1440, doi:10.1175/1520-0493(1976)104<1429:VSOTO>2.0.CO;2.
- Grandpeix, J.-Y., and J.-P. Lafore (2010), A Density Current Parameterization Coupled with Emanuel’s Convection Scheme. Part I: The Models, *J. Atmos. Sci.*, *67*(4), 881–897, doi:10.1175/2009JAS3044.1.
- Grant, L. D., and S. C. van den Heever (2014), Aerosol-cloud-land surface interactions within tropical sea breeze convection, *J. Geophys. Res. Atmos.*, *119*, 8340–8361, doi:10.1002/2014JD021912.
- Grant, L. D., and S. C. van den Heever (2016), Cold pool dissipation, *J. Geophys. Res. Atmos.*, *121*(3), 1138–1155, doi:10.1002/2015JD023813.
- Harrington, J. Y. (1997), The effects of radiative and microphysical processes on simulated warm and transition season Arctic stratus, Colorado State Univ., Fort Collins.
- Hill, G. E. (1974), Factors Controlling the Size and Spacing of Cumulus Clouds as Revealed by Numerical Experiments, *J. Atmos. Sci.*, *31*(3), 646–673, doi:10.1175/1520-0469(1974)031<0646:FCTSAS>2.0.CO;2.
- Horn, B. K. P., and B. G. Schunck (1981), Determining optical flow, *Artif. Intell.*, *17*(1-3), 185–203, doi:10.1016/0004-3702(81)90024-2.
- Jeevanjee, N., and D. M. Romps (2013a), Convective self-aggregation, cold pools, and domain size, *Geophys. Res. Lett.*, *40*(5), 994–998, doi:10.1002/grl.50204.
- Jeevanjee, N., and D. M. Romps (2013b), Convective self-aggregation, cold pools, and domain size, *Geophys. Res. Lett.*, *40*(5), 994–998, doi:10.1002/grl.50204.
- Katona, B. T., A. McGovern, V. Lakshmanan, and A. J. Clark (2014), Automated Identification of Cold Pools in a Convection-permitting model, in *12th Conference on Artificial and*

*Computational Intelligence and its Applications to the Environmental Sciences*, Atlanta, GA.

- Khairoutdinov, M., and D. Randall (2006), High-Resolution Simulation of Shallow-to-Deep Convection Transition over Land, *J. Atmos. Sci.*, 63(12), 3421–3436, doi:10.1175/JAS3810.1.
- Kilpatrick, T. J., and S.-P. Xie (2015), ASCAT observations of downdrafts from mesoscale convective systems, *Geophys. Res. Lett.*, 42(6), 1951–1958, doi:10.1002/2015GL063025.
- Klemp, J. B., and R. B. Wilhelmson (1978), The Simulation of Three-Dimensional Convective Storm Dynamics, *J. Atmos. Sci.*, 35(6), 1070–1096, doi:10.1175/1520-0469(1978)035<1070:TSOTDC>2.0.CO;2.
- Langhans, W., and D. M. Romps (2015), The origin of water vapor rings in tropical oceanic cold pools, *Geophys. Res. Lett.*, 42(18), 7825–7834, doi:10.1002/2015GL065623.
- Li, Z., P. Zuidema, and P. Zhu (2014), Simulated Convective Invigoration Processes at Trade Wind Cumulus Cold Pool Boundaries, *J. Atmos. Sci.*, 71, 2823–2841, doi:10.1175/JAS-D-13-0184.1.
- Lilly, D. K. (1962), On the numerical simulation of buoyant convection, *Tellus*, 14(2), 148–172, doi:10.1111/j.2153-3490.1962.tb00128.x.
- Luo, Y., and Y. Chen (2015), Journal of Geophysical Research : Atmospheres, *J. Geophys. Res. Atmos.*, 120(20), 10,593–10,618, doi:10.1002/2015JD023584.
- Meyers, M. P., R. L. Walko, J. Y. Harrington, and W. R. Cotton (1997), New RAMS cloud microphysics parameterization. Part II: The two-moment scheme, *Atmos. Res.*, 45(1), 3–39, doi:10.1016/S0169-8095(97)00018-5.
- Moncrieff, M. W., and C. Liu (1999), Convection Initiation by Density Currents: Role of

- Convergence, Shear, and Dynamical Organization, *Mon. Weather Rev.*, *127*(10), 2455–2464, doi:10.1175/1520-0493(1999)127<2455:CIBDCR>2.0.CO;2.
- Nicholls, M. E., and R. H. Johnson (1984), A Model of a Tropical Squall Line Boundary Layer Wake, *J. Atmos. Sci.*, *41*(18), 2774–2792, doi:10.1175/1520-0469(1984)041<2774:AMOATS>2.0.CO;2.
- Provod, M., J. H. Marsham, D. J. Parker, and C. E. Birch (2016), A Characterization of Cold Pools in the West African Sahel, *Mon. Weather Rev.*, *144*(5), 1923–1934, doi:10.1175/MWR-D-15-0023.1.
- Qian, L., G. S. Young, and W. M. Frank (1998), A Convective Wake Parameterization Scheme for Use in General Circulation Models, *Mon. Weather Rev.*, *126*(2), 456–469, doi:10.1175/1520-0493(1998)126<0456:ACWPSF>2.0.CO;2.
- Redl, R., A. H. Fink, and P. Knippertz (2015), An Objective Detection Method for Convective Cold Pool Events and Its Application to Northern Africa, *Mon. Weather Rev.*, *143*(12), 5055–5072, doi:10.1175/MWR-D-15-0223.1.
- Ross, A. N., A. M. Tompkins, and D. J. Parker (2004), Simple Models of the Role of Surface Fluxes in Convective Cold Pool Evolution, *J. Atmos. Sci.*, *61*(13), 1582–1595, doi:10.1175/1520-0469(2004)061<1582:SMOTRO>2.0.CO;2.
- Rotunno, R., J. B. Klemp, and M. L. Weisman (1988), A Theory for Strong, Long-Lived Squall Lines, *J. Atmos. Sci.*, *45*(3), 463–485, doi:10.1175/1520-0469(1988)045<0463:ATFSSL>2.0.CO;2.
- Saleeby, S. M., and W. R. Cotton (2004), A Large-Droplet Mode and Prognostic Number Concentration of Cloud Droplets in the Colorado State University Regional Atmospheric Modeling System (RAMS). Part I: Module Descriptions and Supercell Test Simulations, *J.*

- Appl. Meteorol.*, 43(1), 182–195, doi:10.1175/1520-0450(2004)043<0182:ALMAPN>2.0.CO;2.
- Saleeby, S. M., and S. C. van den Heever (2013), Developments in the CSU-RAMS aerosol model: Emissions, nucleation, regeneration, deposition, and radiation, *J. Appl. Meteorol. Climatol.*, 52(12), 2601–2622, doi:10.1175/JAMC-D-12-0312.1.
- Sato, T., H. Miura, M. Satoh, Y. N. Takayabu, and Y. Wang (2009), Diurnal Cycle of Precipitation in the Tropics Simulated in a Global Cloud-Resolving Model, *J. Clim.*, 22(18), 4809–4826, doi:10.1175/2009JCLI2890.1.
- Saxen, T. R., and S. A. Rutledge (1998), Surface Fluxes and Boundary Layer Recovery in TOGA COARE: Sensitivity to Convective Organization, *J. Atmos. Sci.*, 55(17), 2763–2781, doi:10.1175/1520-0469(1998)055<2763:SFABLR>2.0.CO;2.
- Schlemmer, L., and C. Hohenegger (2014), The Formation of Wider and Deeper Clouds as a Result of Cold-Pool Dynamics, *J. Atmos. Sci.*, 71(8), 2842–2858, doi:10.1175/JAS-D-13-0170.1.
- Schlemmer, L., and C. Hohenegger (2016), Modifications of the atmospheric moisture field as a result of cold-pool dynamics, *Q. J. R. Meteorol. Soc.*, 142(694), 30–42, doi:10.1002/qj.2625.
- Seigel, R. B. (2014), Shallow Cumulus Mixing and Subcloud-Layer Responses to Variations in Aerosol Loading, *J. Atmos. Sci.*, 71(7), 2581–2603, doi:10.1175/JAS-D-13-0352.1.
- Seigel, R. B., and S. C. van den Heever (2013), Squall-Line Intensification via Hydrometeor Recirculation, *J. Atmos. Sci.*, 70(7), 2012–2031, doi:10.1175/JAS-D-12-0266.1.
- Seigel, R. B., S. C. Van Den Heever, and S. M. Saleeby (2013), Mineral dust indirect effects and cloud radiative feedbacks of a simulated idealized nocturnal squall line, *Atmos. Chem.*

- Phys.*, 13(8), 4467–4485, doi:10.5194/acp-13-4467-2013.
- Smagorinsky, J. (1963), General circulation experiments with the primitive equations I. The basic experiment, *Mon. Weather Rev.*, 91(3), 99–164, doi:10.1175/1520-0493(1963)091<0099:GCEWTP>2.3.CO;2.
- Srivastava, R. C. (1987), A Model of Intense Downdrafts Driven by the Melting and Evaporation of Precipitation, *J. Atmos. Sci.*, 44(13), 1752–1774, doi:10.1175/1520-0469(1987)044<1752:AMOIDD>2.0.CO;2.
- Terai, C. R., and R. Wood (2013), Aircraft observations of cold pools under marine stratocumulus, *Atmos. Chem. Phys.*, 13(19), 9899–9914, doi:10.5194/acp-13-9899-2013.
- Tompkins, A. M. (2001), Organization of Tropical Convection in Low Vertical Wind Shears: The Role of Cold Pools, *J. Atmos. Sci.*, 58(13), 1650–1672, doi:10.1175/1520-0469(2001)058<1650:OOTCIL>2.0.CO;2.
- Torri, G., and Z. Kuang (2016), A Lagrangian Study of Precipitation-Driven Downdrafts\*, *J. Atmos. Sci.*, 73(2), 839–854, doi:10.1175/JAS-D-15-0222.1.
- Torri, G., Z. Kuang, and Y. Tian (2015), Mechanisms for convection triggering by cold pools, *Geophys. Res. Lett.*, 42(6), 1943–1950, doi:10.1002/2015GL063227.
- Uyeda, H., and D. S. Zrnić (1986), Automatic Detection of Gust Fronts., *J. Atmos. Ocean. Technol.*, 3(1), Mar. 1986, 36–50, doi:http://dx.doi.org/10.1175/1520-0426(1986)003<0036:ADOGF>2.0.CO;2.
- Wakimoto, R. M. (1982), The Life Cycle of Thunderstorm Gust Fronts as Viewed with Doppler Radar and Rawinsonde Data, *Mon. Weather Rev.*, 110(8), 1060–1082, doi:10.1175/1520-0493(1982)110<1060:TLCOTG>2.0.CO;2.
- Wakimoto, R. M., H. V. Murphey, C. A. Davis, and N. T. Atkins (2006), High Winds Generated

- by Bow Echoes. Part II: The Relationship between the Mesovortices and Damaging Straight-Line Winds, *Mon. Weather Rev.*, *134*(10), 2813–2829, doi:10.1175/MWR3216.1.
- Walko, R. L. et al. (2000), Coupled Atmosphere–Biophysics–Hydrology Models for Environmental Modeling, *J. Appl. Meteorol.*, *39*(6), 931–944, doi:10.1175/1520-0450(2000)039<0931:CABHMF>2.0.CO;2.
- Weisman, M. L., and R. Rotunno (2004), “A Theory for Strong, Long-Lived Squall Lines” Revisited, *J. Atmos. Sci.*, *61*(4), 361–382, doi:10.1175/1520-0469(2004)061<0361:ATFSLS>2.0.CO;2.
- Wilbanks, M. C., S. E. Yuter, S. P. de Szoeke, W. A. Brewer, M. A. Miller, A. M. Hall, and C. D. Burleyson (2015), Near-Surface Density Currents Observed in the Southeast Pacific Stratocumulus-Topped Marine Boundary Layer, *Mon. Weather Rev.*, *143*(9), 3532–3555, doi:10.1175/MWR-D-14-00359.1.
- Yokoi, S., M. Katsumata, and K. Yoneyama (2014), Variability in surface meteorology and air-sea fluxes due to cumulus convective systems observed during CINDY/DYNAMO, *J. Geophys. Res. Atmos.*, *119*(5), 2064–2078, doi:10.1002/2013JD020621.
- Young, G. S., S. M. Perugini, and C. W. Fairall (1995), Convective Wakes in the Equatorial Western Pacific during TOGA, *Mon. Weather Rev.*, *123*(1), 110–123, doi:10.1175/1520-0493(1995)123<0110:CWITEW>2.0.CO;2.
- Zipser, E. J. (1977), Mesoscale and Convective–Scale Downdrafts as Distinct Components of Squall-Line Structure, *Mon. Weather Rev.*, *105*(12), 1568–1589, doi:10.1175/1520-0493(1977)105<1568:MACDAD>2.0.CO;2.

Zuidema, P., Z. Li, R. J. Hill, L. Bariteau, B. Rilling, C. Fairall, W. A. Brewer, B. Albrecht, and J. Hare (2012), On Trade Wind Cumulus Cold Pools, *J. Atmos. Sci.*, 69, 258–280, doi:10.1175/JAS-D-11-0143.1.